NAVAL POSTGRADUATE SCHOOL
Monterey, California

THESIS

VARIATIONS ON
AUTOCORRELATION MATCHING
AND THE
SIFT LOCALIZATION ALGORITHM

by

Peter M. de Kooter

March, 1997

Thesis Advisors: Kevin B. Smith
Ching-Sang Chiu

Approved for public release; distribution is unlimited.

REPORT DOCUMENTATION PAGE

Form Approved OMB No. 0704-0188

1. AGENCY USE ONLY *(Leave blank)*	2. REPORT DATE March 1997	3. REPORT TYPE AND DATES COVERED Master's Thesis

4. TITLE AND SUBTITLE
VARIATIONS ON AUTOCORRELATION MATCHING AND THE SIFT LOCALIZATION ALGORITHM

5. FUNDING NUMBERS

6. AUTHOR(S) de Kooter, Peter M.

7. PERFORMING ORGANIZATION NAME(S) AND ADDRESS(ES)
Naval Postgraduate School
Monterey CA 93943-5000

8. PERFORMING ORGANIZATION REPORT NUMBER

9. SPONSORING/MONITORING AGENCY NAME(S) AND ADDRESS(ES)

10. SPONSORING/MONITORING AGENCY REPORT NUMBER

11. SUPPLEMENTARY NOTES The views expressed in this thesis are those of the author and do not reflect the official policy or position of the Department of Defense or the U.S. Government.

12a. DISTRIBUTION/AVAILABILITY STATEMENT
Approved for public release; distribution is unlimited.

12b. DISTRIBUTION CODE

13. ABSTRACT *(maximum 200 words)*

As part of the existing acoustic transient localization program, a feasibility study was performed to apply existing algorithms to signals at higher carrier frequencies. The coherent matching, autocorrelation matching and SIFT algorithms are time domain Matched Field Processing algorithms based on arrival structures for single hydrophone applications. In previous studies, these algorithms were employed only at lower frequencies using ray propagation models to create the replicas with varying success. This study is meant to investigate the performance of the algorithms at higher frequencies, using both the University of Miami Parabolic Equation (UMPE) Model and the Hamiltonian Raytracing Program for the Ocean (HARPO), to give insight into the previously unexplained inconsistent behavior of the algorithms at low frequencies, to improve and optimize existing algorithms, to point out improvements to existing eigenray extraction programs, and to suggest additional signal processing on the signal. Simulations are performed and synthetic signals are generated using both the HARPO and UMPE models. The arrival structures are investigated and the relation between features in the arrival structures for matching and the physical parameters are identified. Some insight into the performance of the SIFT algorithm is gained which relates matching and physical parameters. Simulations lead to improvements and optimization of the algorithms and give insight into the performance at higher frequencies.

14. SUBJECT TERMS Matched Field Processing, Source Localization			15. NUMBER OF PAGES 108
			16. PRICE CODE
17. SECURITY CLASSIFICATION OF REPORT Unclassified	18. SECURITY CLASSIFICATION OF THIS PAGE Unclassified	19. SECURITY CLASSIFICATION OF ABSTRACT Unclassified	20. LIMITATION OF ABSTRACT UL

NSN 7540-01-280-5500

Standard Form 298 (Rev. 2-89)
Prescribed by ANSI Std. 239-18 298-102

Approved for public release; distribution is unlimited.

VARIATIONS ON AUTOCORRELATION MATCHING AND THE SIFT LOCALIZATION ALGORITHM

Peter M. de Kooter
Lieutenant Commander, Royal Netherlands Navy

Submitted in partial fulfillment
of the requirements for the degree of

MASTER OF SCIENCE IN ENGINEERING ACOUSTICS

from the

NAVAL POSTGRADUATE SCHOOL
March 1997

Author: _____
Peter M. de Kooter

Approved by: _____
Kevin B. Smith, Thesis Advisor

_____
Ching-Sang Chiu, Thesis Co-Advisor

_____
Robert M. Keolian, Chairman
Engineering Acoustics Academic Committee

ABSTRACT

As part of the existing acoustic transient localization program, a feasibility study was performed to apply existing algorithms to signals at higher carrier frequencies. The coherent matching, autocorrelation matching and SIFT algorithms are time-domain Matched Field Processing algorithms based on arrival structures for single hydrophone applications. In previous studies, these algorithms were employed only at lower frequencies using ray propagation models to create the replicas with varying success. This study is meant to investigate the performance of the algorithms at higher frequencies, using both the University of Miami Parabolic Equation (UMPE) Model and the Hamiltonian Raytracing Program for the Ocean (HARPO), to give insight into the previously unexplained inconsistent behavior of the algorithms at low frequencies, to improve and optimize existing algorithms, to point out improvements to existing eigenray extraction programs, and to suggest additional signal processing on the signal. Simulations are performed and synthetic signals are generated using both the HARPO and UMPE models. The arrival structures are investigated and the relation between features in the arrival structures for matching and the physical parameters are identified. Some insight into the performance of the SIFT algorithm is gained which relates matching and physical parameters. Simulations lead to improvements and optimization of the algorithms and give insight into the performance at higher frequencies.

TABLE OF CONTENTS

I. INTRODUCTION

Acoustic source localization has been an intensive research issue for the past few decades. Prior to that, passive SONAR was used to obtain an estimate of the source direction and other techniques, such as Target Motion Analysis (TMA), Contact Motion Analysis (CMA) and triangulation, were used to get an estimate of the range to the source. With the introduction of faster computers, other possibilities arose. One of the techniques that was developed is known as Matched Field Processing (MFP). The MFP process consists of systematically placing a synthetic source at each point in a search grid and comparing the signal received from all the synthetic sources with the signal received from the true source. When the synthetic source location and the true source location match, the correlation of the true and the synthetic received signals should be maximum. Most of the work in this field has been done with array receivers and narrow band signals. The project-in-hand concerns itself with the case of a single receiver hydrophone and broadband signals.

The objective of this study is an examination of the influence of the physics mismatch in the prediction of the acoustic propagation on a number of MFP algorithms for a single hydrophone receiver and a transient-like point source. A time-domain signal autocorrelation matching is performed to produce the ambiguity surface for the localization. A full wave, parabolic equation model is employed to produce a synthetic signal and a reciprocal prediction to provide a baseline for the correlation. Predictions from a ray-based propagation model are then matched to the synthetic signal. By comparing this ambiguity surface with the baseline, the influence of the physics mismatch due to the ray predictions

can be quantified. Several aspects of the ray model can be independently affected providing information of model degradation on localization performance. A secondary but not less important objective is to suggest directions for future research beyond the present available algorithms.

The remainder of this thesis consists of five chapters. Chapter II describes the propagation models and arrival structure synthesis. Chapter III describes the matching algorithms and the influence of physical parameters on these algorithms. Chapter IV describes the setup of the experiments and the results of the autocorrelation matching and the approximate autocorrelation matching. Chapter V describes the issues which were encountered during the research and were not investigated, but which may lead to more insight into the performance of present algorithms or lead to more robust algorithms. Chapter VI presents the conclusions of the study. In the Appendix, a derivation for a frequency based analogue of a generalized beamformer for a single hydrophone is presented, and the relationship to autocorrelation matching is briefly discussed.

II. PROPAGATION MODELS AND ARRIVAL STRUCTURE SYNTHESIS

Propagation models and in particular the relation of their parameters to physical parameters form a major part of the basis of this research. The step from the output of the propagation models to an arrival structure from another important part. This is also the step where some of the major approximations are made. For this research, two propagation models have been used: a full wave parabolic equation model and a Hamiltonian raytracing propagation model. The models are based on the same wave equation but different assumptions are made to generate an approximate solution. We begin with the homogeneous wave equation for the acoustic pressure in a medium with sound speed $c(\vec{x})$ and density $\rho(\vec{x})$, (Jensen et al. 1994)

$$\rho(\vec{x})\nabla\cdot\left(\frac{\nabla p(\vec{x},t)}{\rho(\vec{x})}\right)-\frac{1}{c(\vec{x})^2}\frac{\partial^2 p(\vec{x},t)}{\partial t^2}=S(\vec{x}_s,t). \qquad (1)$$

Assuming a harmonic solution, $p(\vec{x},t)=p(\vec{x})e^{i\omega t}$, leads to the corresponding Helmholtz equation

$$\rho(\vec{x})\nabla\cdot\left(\frac{\nabla p(\vec{x})}{\rho(\vec{x})}\right)-\frac{\omega^2 p(\vec{x})}{c^2(\vec{x})}=S_\omega(\vec{x}_s), \qquad (2)$$

where S is the source function and p is pressure, which are generally complex. The right-hand term is zero when the source is not included, which is true for the major part of the

ocean. For a fixed density and a range independent environment the formulas could even be more simplified to

$$\left(\nabla^2 - \frac{\omega^2}{c^2(\vec{x})}\right) p(\vec{x}) = 0. \tag{3}$$

Although the models incorporate more features and are based on generalized versions of the above formulas (e.g., including currents) those features are not used in this project.

A. HAMILTONIAN RAYTRACING

Raytracing or geometrical acoustics assumes that sound waves travel along geometric paths called rays. Each 'ray' travels along a certain path which is dictated by the local sound speed and, where appropriate, boundary interactions. Assuming a constant density, we assume a solution of the form (Jensen et al., 1994)

$$p(\vec{x}) = e^{i\omega\tau(\vec{x})} \sum_{j=0}^{\infty} \frac{A_j(\vec{x})}{(i\omega)^j}, \tag{4}$$

which represents a ray series solution. This form, although in general divergent, provides an asymptotic approximation to the exact solution of the Helmholtz equation in certain cases. The series term expresses the frequency dependence of the amplitude.

Usually only the first term in the series solution is used in the derivation. The governing equations for the ray theory are then

$$\nabla\tau(\vec{x})|^2=\frac{1}{c^2(\vec{x})}, \tag{5}$$

$$2\nabla\tau(\vec{x})\cdot\nabla A_0(\vec{x})+\nabla^2\tau(\vec{x})A_0=0, \tag{6}$$

and

$$2\nabla\tau(\vec{x})\cdot\nabla A_j(\vec{x})+\nabla^2\tau(\vec{x})A_j=-\nabla^2A_j(\vec{x}) \quad j=1,2,....., \tag{7}$$

where τ is the travel time phase and A is the amplitude. The first equation is known as the eikonal equation. It determines the local direction of the phase front and, as rays travel perpendicular to phase fronts, it determines the ray paths. The second and latter equations are called the transport equations of which only the first is commonly used. This is the same as taking a first order approximation instead of a series solution. The second and latter equations determine the amplitude along the ray path. Furthermore, the expressions above make use of the approximations

$$\omega\gg\nabla c(\vec{x}) \quad and \quad \frac{\nabla^2A}{k_0^2A}\ll 1$$

such that variations of the sound speed and variations in amplitude occur over much larger scales than a wavelength. The neglect of higher order terms in the above solution leads to the assumption that the energy is conserved within a ray tube (higher order terms include leakage) and leads to a break down of the transport equation at or near focal points (caustics).

In geometric acoustics, a ray behaves much like a particle. Therefore, Hamiltonian theory can be applied to the propagation of sound (Lighthill, 1978). The first order ray equations derived from the eikonal equation can be written as

$$\frac{d\vec{x}}{ds}=k(\vec{x})^{-1}\vec{k}(\vec{x}), \tag{9}$$

$$\frac{d\vec{k}(\vec{x})}{ds}=k_0\nabla n(\vec{x}), \tag{10}$$

$$n=\frac{c_0}{c(\vec{x})}, \tag{11}$$

where s is the path length, $k(\vec{x})=\frac{\omega}{c(\vec{x})}$ is the wave number, $k_0=\frac{\omega}{c_0}$ is the reference wave number, c_0 is the reference sound speed and n is the acoustical index of refraction. The equivalent Hamiltonian equations can be written as

$$\frac{d\vec{x}}{d\tau}=\nabla_{\vec{k}}H(\vec{x},\vec{k},\omega,t), \tag{12}$$

$$\frac{d\vec{k}}{d\tau} = -\nabla H(\vec{x},\vec{k},\omega,t), \tag{13}$$

$$H(\vec{x},\vec{k},\omega,t) = \omega^2 - c^2(\vec{x})k^2 = 0, \tag{14}$$

and

$$\tau = \frac{-t}{4\pi f}. \tag{15}$$

In this information, the Hamiltonian is zero along the ray path. For this project, time and frequency dependence of the Hamiltonian are neglected (i.e., no volume attenuation, currents, or changing environments). All frequency dependent features such as boundary interactions are calculated in the postprocessing. Although the Hamiltonian is a constant of the motion in this formulation, the number of degrees of freedom (3) exceeds the number of constants. In general, ray paths are then chaotic (Smith et al., 1992). However, in this project, the environment is two dimensional and range-independent, and all the ray paths are regular.

B. HAMILTONIAN RAYTRACING PROGRAM FOR THE OCEAN (HARPO)

The raytracing program used for this thesis is the Hamiltonian Raytracing Program for the Ocean (HARPO). HARPO is written in Fortran and its roots go back to a program

written by Dudrak (1961). It has since been updated by many different people. The program treats the ocean as a continuous changing environment and not as a large number of stratified segments thereby avoiding effects such as false caustics. Of the ray parameters, only the ray paths and the travel times are computed by the HARPO program. Amplitude and path length are determined in the postprocessing.

The heart of the program is a fourth-fifth order Adams Moulton predictor corrector algorithm to integrate the Hamiltonian equations along the ray path. The accuracy of the integration process and the spacing of the initial ray fan are extremely important parameters for the calculation of the eigenray parameters. Comparisons with analytical results of travel times have indicated that the calculations are highly accurate with phase errors $\leq \pi/100$ up to 10 km at 1 kHz.

Two features in the design of the program make the standard output not particularly suitable for a straightforward eigenray extraction routine. The rays are referenced to a spherical coordinate system and the points along the ray are not equally spaced in range. This hampers some of the necessary improvements for eigenray extractions close to the boundaries, and makes it necessary to use a local Cartesian coordinate system to avoid complicated formulations. In what follows, a two-dimensional environment, specifying range and depth positions (r,z) will be assumed.

C. EIGENRAY EXTRACTION

Eigenrays are rays that connect source and receiver. The number of eigenrays is generally quite large. Usually only a small number has enough amplitude to be important, however. Eigenray extraction programs are, in a general sense, root solvers. In Fig. 1, a plot of launch angle versus depth at some finite range, it is clearly shown that the eigenrays for a given range and depth are the roots for that depth of the curve given in the figure.

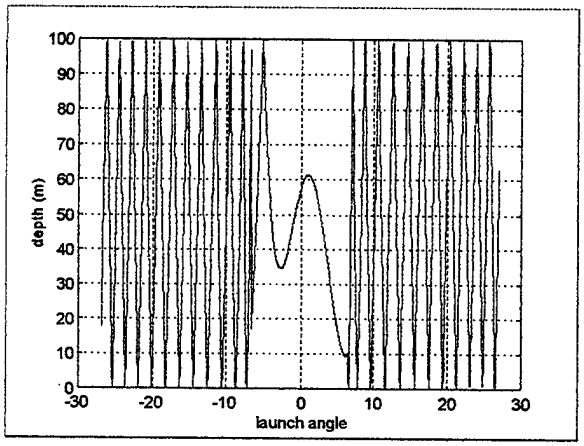

Figure 1 Launch angle versus depth plot at a certain range.

As the output of HARPO is not organized in a convenient range/depth grid, the process of finding the eigenrays is more involved. An eigenray extraction program developed in Matlab (ray3d.m) by Chiu deals with this matter. The program selects the rays with a (local) minimum vertical distance to the receiver location out of the total fan of rays and calculates

the ray parameters by a third order polynomial interpolation using these selected rays and adjacent rays. No retracing of the eigenrays is done. The eigenray parameters calculated by the program are: phase travel time τ, the path length s, the local sound speed c, the local sound speed gradient ∇c, the local direction of the ray θ, the launch angle θ_0, the amplitude due to reflections, the phase shift due to reflections and turning points, and the amplitude due to geometrical spreading.

The amplitude along the ray is not calculated in HARPO, but in the eigenray extraction routine based on the equivalent WKB formulation of the ray solution. The calculation is based on the conservation of power within a ray tube. The formula based on the assumption of a point source, used for the amplitude calculation is (Ziomek, 1995)

$$|P_f(r,z)|^2 = |P_f(r_1,z_1)|^2 \frac{\rho_0(r,z)c(r,z)}{\rho_0(r_1,z_1)c(r_1,z_1)} \frac{R_0^2 \cos(\beta_0)}{r|\sin(\beta(r,z))dr_\perp/d\beta_0|}, \qquad \textbf{(16)}$$

where $|P_f(r,z)|$ is the pressure amplitude at the gridpoint, $|P_f(r_1,z_1)|$ is the pressure amplitude at 1 m (which can be related to the source level), $\rho_0(r,z)$ is the density at the gridpoint, $\rho_0(r_1,z_1)$ is the density at 1 m from the source, $c(r,z)$ is the sound speed at the gridpoint, $c(r_1,z_1)$ is the reference sound speed at 1 m, R_0=1 m, β_0 is the launch angle of the eigenray, r is the horizontal range from the source of the gridpoint, and $dr_\perp$ relates to the distance perpendicular to the direction of the wavefront. We can rewrite this using

$$a=\frac{|P_f(r,z)|^2}{|P_f(r_1,z_1)|^2},$$

$$\rho_0(r_1,z_1)=\rho_0(r,z), \qquad (17)$$

$$R_0=1,$$

$$\delta=r\sin(\beta),$$

and arrive at

$$a=\frac{c(r,z)}{c(r_1,z_1)}\ \frac{\cos(\beta_0)}{r\delta/d\beta_0}. \qquad (18)$$

This formulation is known to produce infinite amplitudes at and near turning and focal points. However, the numerical implementation used here prevents the amplitude from blowing up. Ordinarily the $\delta/d\beta_0$ is calculated using the selected ray (which is locally closest to the gridpoint). When this ray is too close, the fan is opened up a little. The same is done when the amplitude exceeds the cylindrical spreading amplitude.

The routines for the reflection coefficients are based on plane wave reflection coefficients. The surface reflection coefficient is set to unity, with a 180 degrees phase shift, $R_s=e^{-i\pi}$, while the bottom reflection coefficient is calculated including the sediment attenuation α (dB/Hz/km) by

$$c_{c,i}=\frac{c_b^2}{2\pi f}\alpha\frac{f}{1000}20\log_{10}(e), \tag{19}$$

$$\theta_b=\cos^{-1}\left(\frac{(c_b+c_{b,i})}{c}\cos(\theta_i)\right), \tag{20}$$

so

$$R_b=\frac{\rho_b(c_b+ic_{b,i})\sin(\theta_i)-\rho c\sin(\theta_b)}{\rho_b(c_b+ic_{b,i})\sin(\theta_i)+\rho c\sin(\theta_b)}. \tag{21}$$

Written in terms of an amplitude and a phase this leads to

$$R_b=|R_b|e^{i\phi_b}, \tag{22}$$

where

$$|R_b|=\sqrt{\frac{(\rho_b c_b\sin(\theta_i)-\rho c\sin(\theta_b))^2+(\rho_b c_{b,i}\sin(\theta_i))^2}{(\rho_b c_b\sin(\theta_i)+\rho c\sin(\theta_b))^2+(\rho_b c_{b,i}\sin(\theta_i))^2}}, \tag{23}$$

and

$$\phi_b=\tan^{-1}\frac{\rho_b c_{b,i}\sin(\theta_i)}{\rho_b c_b\sin(\theta_i)-\rho c\sin(\theta_b)}-\tan^{-1}\frac{\rho_b c_{b,i}\sin(\theta_i)}{\rho_b c_b\sin(\theta_i)+\rho c\sin(\theta_b)}. \tag{24}$$

At ray turning points, we can express the phase change in terms of an equivalent "reflection coefficient", i.e., $R_t = e^{-i\pi/2}$. The total phase for selected rays (which are representative of the eigenrays) is then calculated as

$$\theta = -N_t\pi/2 - N_s\pi - \sum_{j=1}^{N_b} \phi_{b,j}, \tag{25}$$

where the number of turning points, surface reflections and bottom reflections are given by N_t, N_s and N_b respectively.

The phase of a ray changes according to reflections, refractions and travel time. Refractions close to the surface and close to the bottom may not cause a discrete $-\pi/2$ phase change but something between $-\pi/2$ and the phase change due to the reflection. Furthermore, the position in range is not strictly localized at the refracted points. This together with the fact that small errors accumulate per bounce and may give the phase of a ray a random component which can be quite large.

The estimation of the amplitude of a ray is also numerically difficult. Opening up the ray fan as discussed before does not give you a true estimate but rather a conservative estimate due to the averaging caused by opening up the ray fan. However, travel times are estimated very accurately. Still, at high frequencies, small errors may lead to unacceptable phase errors. For ranges and frequencies considered in this project, we do not expect travel time errors to be significant.

D. ARRIVAL STRUCTURE SYNTHESIS FROM EIGENRAY DATA

Several different approaches have been used to derive arrival structures from eigenray data for different localization algorithms. The important parameters used in the synthesis are

τ_n	eigenray travel time (relative and absolute travel time),
θ	eigenray phase (due to reflections and refractions),
f_c	carrier frequency (which together with the travel time may account for a major part of the phase),
a_n	eigenray amplitude, and
s(t),S(f)	source function (pulse/transient) in time or frequency domain (real or complex).

For the synthesis, the ocean is considered as a linear time invariant filter causing a time delay and a phase shift. The total amplitude and phase contribution due to the reflections and refractions for each eigenray can be written as

$$R_n(f) = \left[\prod_{j=1}^{N_b} R_{b,j}(f)\right]\left[\prod_{j=1}^{N_s} R_{s,j}(f)\right]\left[\prod_{j=1}^{N_t} R_{t,j}(f)\right] = |R_n(f)| e^{-i\theta_n(f)}, \tag{26}$$

where the product in Eq. (25) represents the accumulated effects of multiple reflections and refractions and the last equation specifies the conjugation for negative frequencies. For this

$$\theta(f)=\begin{cases}\theta(f) & f>0\\ -\theta(-f) & f<0\end{cases} \tag{27}$$

project we assume that R_n is frequency independent. The frequency response of a real received signal from an individual arrival can then be written as

$$Y_n(f)=H_n(f)\ X(f) \tag{28}$$

where

$$H_n(f)=a_n(f)\ R_n\ T_n(f) \tag{29}$$

is the complex frequency domain transfer function, a_n represents the geometrical amplitude factor, and T_n represents the phase change due to the time delay. Note that $Y_n(f)=Y_n^*(-f)$ since the time domain signal is real. We assume that the amplitude factor is also frequency independent and the delay factor can be written as

$$T_n(f)=e^{-i2\pi f\tau_n}. \tag{30}$$

We can now write $Y_n(f)$ as

$$Y_n(f)=a_n\ R_n\ e^{-i\theta_n}e^{-i2\pi f\tau_n}X(f). \tag{31}$$

In the time domain, this can be written as

$$y_n(t)=a_n\ R_n \int_{-\infty}^{\infty} X(f)e^{-i\theta_n}e^{i2\pi f(t-\tau_n)}df. \tag{32}$$

The arrival structure is then defined as the sum over all eigenrays of the individual arrivals i.e.,

$$y(t)=\sum_{n=1}^{N} y_n(t). \tag{33}$$

For some applications, it may be easier to first sum in the frequency domain,

$$Y(f)=\sum_{n=1}^{N} Y_n(f), \tag{34}$$

and then transform the results to the time domain,

$$y(t)=\int_{-\infty}^{\infty} Y(f)e^{i2\pi ft}df. \tag{35}$$

These two approaches should be equivalent.

For some localization algorithms, it may be preferable to perform all the calculations in the frequency domain. For bandpass signals, it might be desirable to cast it in terms of the preenvelope or complex envelope of the received signal. This results in a few minor changes in the formulas. Specifically, we treat the time domain signal as complex (i.e., neglect the negative portion of the spectrum) and define the basebanded frequency response as

$$\tilde{Y}_n(f)=\tilde{H}_n(f+f_c)\ \tilde{X}(f) \tag{36}$$

or

$$\tilde{Y}_n(f)=a_n\ R_n\ \tilde{X}(f)\ e^{-i\theta_n}e^{-i2\pi f_c\tau_n}e^{-i2\pi f\tau_n}. \tag{37}$$

If we write the complex source function as

$$\tilde{x}(t)=F^{-1}\{\tilde{X}(f)\} \tag{38}$$

where

$$\tilde{x}(t)=\{x(t)+i\hat{x}(t)\}e^{-i2\pi f_c t} \tag{39}$$

then the complex received signal of a single eigenray can be written as

$$\begin{aligned}\tilde{y}(t)&=\tilde{x}(t-\tau_n)e^{-i\theta_n-i2\pi f_c\tau_n}\\&=\tilde{x}(t-\tau_n)\cos(\theta+2\pi f_c\tau_n)-i\tilde{x}(t-\tau_n)\sin(\theta+2\pi f_c\tau_n)\end{aligned} \tag{40}$$

where f_c is the carrier frequency or center frequency of the pass band.

Another way to write the received signal, which was used in previous simulations and which is especially applicable to low pass signals, can be derived starting from the preenvelope (no base banding) of the source function

$$\tilde{x_p}(t)=x(t)+i\hat{x}(t), \tag{41}$$

where $\hat{x}(t)$ is the Hilbert transform of the real source function $x(t)$, and the frequency spectrum of the preenvelope $\tilde{x}_p(t)$ is the same as that of $x(t)$ but with the negative frequencies discarded. From the preenvelope of the received signal

$$\tilde{y}_n(t)=\tilde{x}_p(t-\tau_n)e^{-i\theta_n}, \tag{42}$$

the real received signal can be described by

$$\begin{aligned} y_n(t) &= Re\{\tilde{x}_p(t-\tau_n)e^{-i\theta_n} \\ &= x(t-\tau_n)\cos(\theta_n)+i\hat{x}(t-\tau_n)\sin(\theta_n). \end{aligned} \tag{43}$$

E. THE PARABOLIC EQUATION MODEL

The parabolic equation model used here is based on an approximation to the Helmholtz description of the wave equation in a cylindrical coordinate system. The majority of the ocean environment is well suited for a description in cylindrical coordinates. Assuming a time harmonic solution, the Helmholtz equation in cylindrical coordinates takes the form (see, for example, Jensen et al., 1994)

$$\frac{1}{r}\frac{\partial}{\partial r}\left(r\frac{\partial p_f(r,z,\phi)}{\partial r}\right)\frac{1}{r^2}\frac{\partial^2 p_f(r,z,\phi)}{\partial \phi^2}+\frac{\partial^2 p_f(r,z,\phi)}{\partial z^2}+k_0^2 n^2(r,z,\phi)p_f(r,z,\phi)=-4\pi P_0\delta(\vec{r}-\vec{r}_s), \quad \textbf{(44)}$$

where

$$p(r,z,\phi,f,t)=p_f(r,z,\phi)e^{2\pi ft}, \quad \textbf{(45)}$$

$k_0=\frac{\omega}{c_0}$ is a reference wave number and the acoustic index of refraction is defined by

$$n=\frac{c_0}{c(r,z,\phi)}. \quad \textbf{(46)}$$

As energy is primarily radiating outward from the source, $p_f(r,z,\phi)$ can be approximated by

$$p_f(r,z,\phi)=\Psi_f(r,z,\phi)H_0^1(k_0 r), \quad \textbf{(47)}$$

where $\Psi_f(r,z,\phi)$ is a slowly varying envelope and $H_0^1(k_0 r)$ is the outward going Hankel function. In the far field, the Hankel function takes the form of an outward going plane wave and so we define

$$p_f(r,z,\phi)=\frac{1}{\sqrt{(r)}}\Psi(r,z,\phi)e^{-ik_0 r}. \quad \textbf{(48)}$$

Substituting this into Eq. (43) yields

$$\frac{\partial^2\Psi}{\partial r^2}+i2k_0\frac{\partial\Psi}{\partial r}+\frac{1}{r^2}\frac{\partial^2\Psi}{\partial\phi^2}+\frac{\partial^2}{\partial z^2}+\left(k_0^2(n^2-1+\frac{1}{4k_0r^2}\right)\Psi=0, \tag{49}$$

where the source function on the right-hand side has been dropped. Neglecting the azimuthal coupling and the near field terms and assuming that Ψ is a slowly varying function with range, we arrive at

$$\frac{\partial\Psi}{\partial r}=\frac{i}{2k_0}\frac{\partial^2\Psi}{\partial z^2}+\frac{ik_0}{2}(n^2-1)\Psi. \tag{50}$$

Defining the operators

$$T_{op}=-\frac{1}{2}\left(-ik_0^{-1}\frac{\partial}{\partial r}\right)^2 \tag{51}$$

and

$$U_{op}=-\frac{1}{2}(n^2-1), \tag{52}$$

this can be written as

$$ik_0^{-1}\frac{\partial\Psi}{\partial r}=(T_{op}+U_{op})\Psi. \tag{53}$$

With the operators defined above, this constitutes what is commonly referred to as the "standard" parabolic equation (Tappert, 1977). For this work, we have employed the higher order "wide angle" parabolic equation (Thomson and Chapman, 1983) with operators defined by

$$T_{WAPE}=\frac{\partial^2}{\partial z^2}\left[\left(1+\frac{\partial^2}{\partial z^2}\right)^{1/2}+1\right]^{-1}, \tag{54}$$

and

$$U_{WAPE}=-(n-1), \tag{55}$$

The parabolic equation model that was used for this project is the University of Miami Parabolic Equation model (Smith and Tappert, 1994). A split-step Fourier algorithm is used to numerically integrate the solution in range. This involves alternatively applying the U_{op} and the T_{op} operators in the z-domain and the k_z-domain, respectively, where each operator is simply a scalar multiplier. The algorithm for stepping in range from r to $r + \Delta r$ can then be succintly expressed as

$$\Psi(r+\Delta r,z)=e^{ik_0\Delta r U_{op}(r,z)}\times FFT\{e^{-ik_0\Delta r\hat{T}_{op}(r,k_z)}\times[FFT(\Psi^*(r,z))]^*\}, \tag{56}$$

where the wide angle $\hat{T}_{op}$ operator in the k_z-space is defined as

$$\hat{T}_{WAPE}(k_z)=1-\left[1-\left(\frac{k_z}{k_0}\right)^2\right]^{1/2}. \quad \textbf{(57)}$$

The output of the model is in the form of the field functions Ψ (magnitude and phase) and has been referenced to a source strength of 1 μP at 1 m. The field is only computed at discrete points and the spacing in depth and range are the primary parameters that determine the accuracy of the results. The wavelength of interest in this study is 1.5-2 m and the grid spacing used is 40 cm in depth and 50 cm in range. Note that the grid size is ~ λ/4 which is necessary to obtain the highest accuracy up to ± 90 degrees propagation angles. In general, we would expect that a courser grid size would produce similar results in shallow water environments where propagation angles are often limited to < 15 degrees.

F. PE ARRIVAL STRUCTURES

The pressure is defined in terms of the PE field function by

$$p(r,z,f)=\frac{P_0}{\sqrt{r}}R_0 e^{ik_0 r}\Psi(r,z,f), \quad \textbf{(58)}$$

where P_0 is the amplitude of the source pressure measured at R_0=1 m. The broadband results were obtained by running the model multiple times for all discrete frequencies in the

bandwidth under consideration and then performing a Fourier synthesis to yield travel time results. Assuming a normalized source amplitude, the complex arrival structure of the pressure field can then be written as

$$p(r,z,t)=\int_{-\infty}^{\infty} p(r,z,f)e^{i2\pi ft}dt$$
$$=\frac{1}{\sqrt{r}}\int_{-\infty}^{\infty} e^{ik_0 r}\Psi(z,r,f)e^{i2\pi ft}df. \qquad \textbf{(59)}$$

Since $e^{ik_0 r}=e^{i2\pi f\frac{r}{c_0}}$, this phase factor can be neglected by defining the reduced time $T=t-\frac{r}{c_0}$ such that

$$p(r,z,T)=\frac{1}{\sqrt{r}}\int_{-\infty}^{\infty}\Psi(z,r,\phi)e^{i2\pi fT}df. \qquad \textbf{(60)}$$

Note that using a reduced time has no influence on the autocorrelation function.

III. LOCALIZATION ALGORITHMS

The Transient Localization Project at the Naval Postgraduate School has in recent years studied different localization algorithms for the scenario of one receiver hydrophone and a point source. All the routines were based on fundamental concepts of generalized correlation functions described in Bendat and Piersol, 1996 and most of them are described in Miller et al., 1996.

Localization algorithms may be considered generalized beamformers in which the plane wave replicas have been replaced by more complicated replicas of the acoustic propagation (e.g., modes, beams, or the vertical pressure field). The algorithms, usually referred to as processors, are in most cases based on a Hermitian quadratic product. The exact form is determined by the constraints that are put on the processor output.

The main algorithm developed previously developed at the Naval Postgraduate School was the Signal Integration Filtering in Time (SIFT) algorithm which is a form of time domain autocorrelation matching (Benson, 1995). This algorithm had considerable success in the localization experiments in the Barents Sea (Benson, 1995). Although the results were favorable, there were still questions about the influence of environmental model parameters and acoustic (ray) model parameters on the results.

All the localization algorithms described below are described for the single hydrophone case but can easily be extended to an array of hydrophones. The source is described as an omnidirectional point source and the receiver is a single omnidirectional hydrophone.

All localization algorithms are based on matching the received signal with a replica. Replicas are simulated received signals of synthetic sources at a large number of gridpoints in a search space. When the propagation model is 100% correct and the synthetic and real source functions are equal, the real and synthetic received signal should exactly match when the real and synthetic source positions coincide. Results of the localization are usually represented as an ambiguity surface. All MFP algorithms are based on this principle in some form. Using the reciprocity principle reduces the amount of work to a manageable size, and makes localization possible in a reasonable and operational feasible time. The reciprocity principle states that in an environment without time variations (e.g., currents) the acoustic pressure at location B from an omnidirectional source at location A and the acoustic pressure at A from an equivalent source at B are inversely proportional to the densities at A and B. If we assume the densities are the same at A and B, we may interchange hydrophone and source locations and thereby reduce the amount of work.

A. FULLY COHERENT LOCALIZATION

Fully coherent localization is based on a normalized time domain cross correlation of a signal and the set of replicas. Given a received signal

$$r(t)=\int_{-\infty}^{\infty}R(f)e^{i2\pi ft}df, \tag{61}$$

and predicted replicas

$$p(t)=\int_{-\infty}^{\infty}P(f)e^{i2\pi ft}df, \tag{62}$$

the cross correlation is given by

$$C_{RP}(\tau)=\frac{\int_{-\infty}^{\infty}R^{*}(f)P(f)e^{i2\pi f\tau}df}{\sqrt{\int_{-\infty}^{\infty}|R(f)|^{2}df\int_{-\infty}^{\infty}|P(f)|^{2}df}}. \tag{63}$$

In the frequency domain, the replicas may be represented by

$$P(f)=H(f)S(f) \tag{64}$$

where $H(f)$ represents the propagation model and $S(f)$ represents the source function of the replica, or template signal.

The maximum of the peak will reflect the degree in which the modeled signal matches the real received signal. Only the peak value of this cross correlation is utilized. When the synthetic and real source coincide and the ocean model is 100% correct the value should be 1. This method suffers from a number of flaws. $R(f)$ and $P(f)$ are in general complex and their phase is very dependent on the ocean model parameters. (We neglect the source function dependence which will be discussed in the chapter on future work). A phase mismatch of 90 degrees at a given point will produce a zero cross-correlation. Such a mismatch at 1000 Hz can easily be caused by small sound speed or bathymetry errors, so this method does not seem to be viable for practical situations. Applying the algorithm at basebanded signals does not solve the phase problem.

B. SEMI-COHERENT LOCALIZATION

To avoid the problems with phase mismatch, which are more likely at high frequencies, a semi coherent approach can be taken. In this approach, the absolute value of the time domain replicas and the received signal is passed through a lowpass filter. This is similar to broadband demodulation. The matching algorithm is then performed on the low pass signal, i.e.,

$$R'(f)=H_{LP}(f)\int_{-\infty}^{\infty}\left|\int_{-\infty}^{\infty}R(f')e^{i2\pi f't}df'\right|e^{-i2\pi ft}dt \tag{65}$$

$$P'(f)=H_{LP}(f)\int_{-\infty}^{\infty}\left|\int_{-\infty}^{\infty}P(f')e^{i2\pi f't}df'\right|e^{-i2\pi ft}dt \tag{66}$$

and so

$$C_{RP}(\tau)=\frac{\int_{-\infty}^{\infty}R'(f)P'(f)e^{j2\pi f\tau}df}{\sqrt{\int_{-\infty}^{\infty}|R'(f)|^2df\int_{-\infty}^{\infty}|P'(f)|^2df}} \tag{67}$$

The match is again found at the maximum of $C_{RP}(\tau)$. Previously this algorithm was used without much success (Miller et al. 1996) and will not be used here. However, careful analysis of the effects of errors in the parameters of the environment or the eigenrays on the arrival structures may shed some light on the poor results.

The replica $P'(f)$ shows that the largest amplitudes coincide with the earliest arrivals. This portion of the signal therefore provides the largest contribution to the result of the match. However the amplitudes of these arrivals are most prone to error due to poor estimation of the amplitudes of refracted rays which form the largest part of the initial arrivals. The semi-coherent algorithm may avoid the phase errors but amplifies the

amplitude errors. An improvement could be to normalize the amplitude of the replica. A number of other improvements could also be made, such as sampling at the arrival times of the individual rays, or clipping the template.

C. TIME-DOMAIN AUTOCORRELATION MATCHING

One of the problems with the previous algorithms is the lack of an absolute time reference. The time domain autocorrelation matching algorithm removes the absolute time reference from the received signal and the replica. The autocorrelation of the received signal is defined as

$$G_{RR}(\tau) = \int_{-\infty}^{\infty} R^*(f)R(f)e^{i2\pi f\tau}df \qquad \textbf{(68)}$$

and the autocorrelation of the replica is similarly

$$G_{PP}(\tau) = \int_{-\infty}^{\infty} P^*(f)P(f)e^{i2\pi f\tau}df. \qquad \textbf{(69)}$$

The autocorrelation matching can then be computed by

$$A_{RP}=\frac{\sum_{-\infty}^{\infty} G_{RR}(\tau)G_{PP}(\tau)}{\sqrt{\sum_{-\infty}^{\infty}|G_{RR}(\tau)|^2\sum_{-\infty}^{\infty}|G_{PP}(\tau)|^2}}. \tag{70}$$

or in the frequency domain, using

$$G_{RR}(f)=\int_{-\infty}^{\infty} G_{RR}(\tau)e^{-i2\pi f\tau}df, \tag{71}$$

$$G_{PP}(f)=\int_{-\infty}^{\infty} G_{PP}(\tau)e^{-i2\pi f\tau}df \tag{72}$$

then

$$A_{RP}=\frac{\sum_{-\infty}^{\infty} G_{RR}^{*}(f)G_{PP}(f)}{\sqrt{\sum_{-\infty}^{\infty}|G_{RR}(f)|^2\sum_{-\infty}^{\infty}|G_{PP}(f)|^2}}. \tag{73}$$

Originally the matching was designed for the real signals in the time domain.

There are two primary advantages of autocorrelation matching. First the influence of noise tends to concentrate near zero lag values. By cutting out values around zero lag, the

effect of noise is significantly reduced. Cutting out values around zero lag also has a distinct effect on the contrast of the ambiguity surface as can be seen in Fig. 2. Matching values now range from -1 to 1. Values between -1 and 0 are neglected in all subsequent plots. The second advantage is the removal of any absolute time of reference. Only relative arrival times of separate multipaths are compared.

Throughout most of this project, the received signals will be generated synthetically using the PE model. Replicas were generated using the same PE model for various environments to determine the optimum number of lag values near zero to remove. The

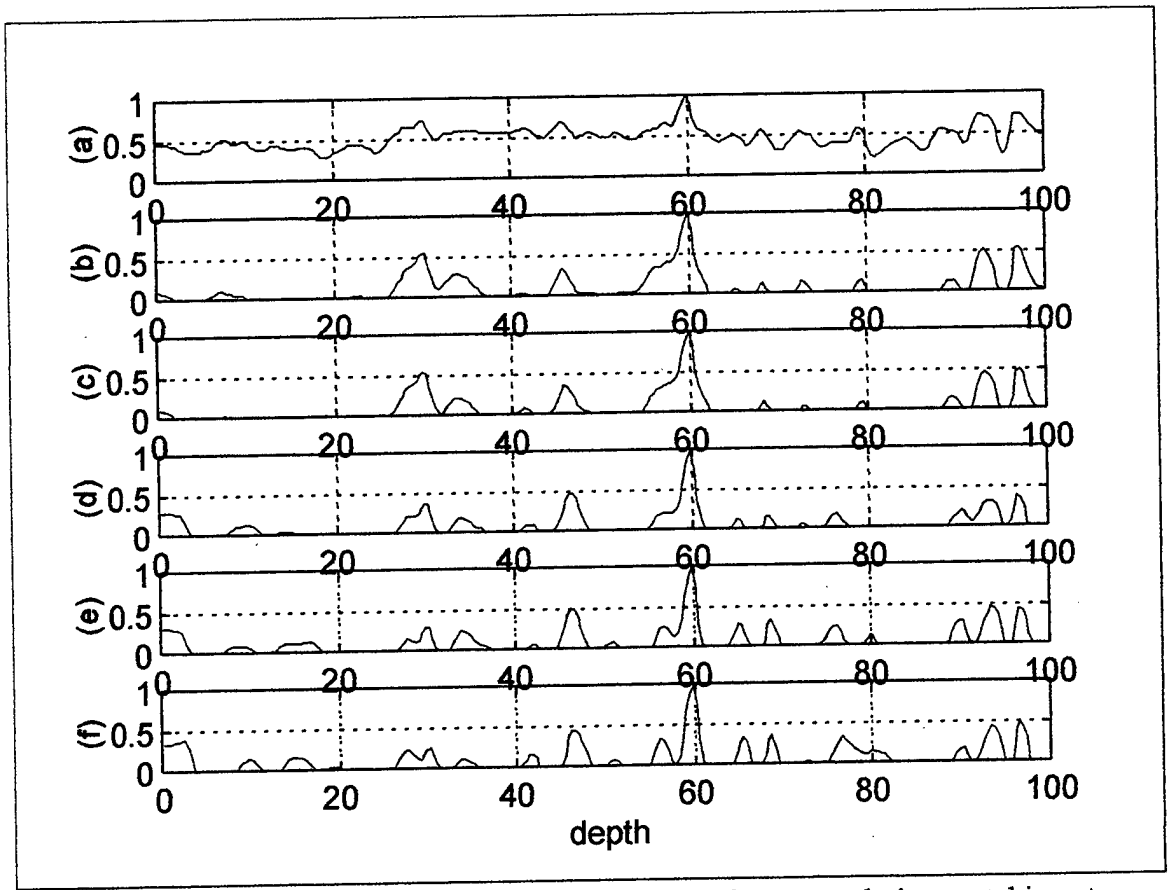

Figure 2 Effect of notching out near zero lag values of autocorrelation matching at a certain range. Plots (a) - (f) show increasing number of notched out values.

results indicate that this number depends on the shape of the source signal and therefore on the bandwidth. Furthermore, where it has a positive effect on the contrast, it has a negative effect on the footprint size. For example, by removing seven points near zero lag (zero lag plus three at positive and three at negative lags) for a negative gradient environment, the footprint is reduced from about five meters in depth to about two and a half meters in depth. The footprint size does not seem to be reduced further when more points than the optimum number of points are removed. However, the removal of more points begins to degrade the performance by increasing the level of false peaks (sidelobes). Note that the removal of near zero lag points in the time domain is equivalent to removing the mean and lowest order trends from the frequency domain. We found that the removal of points corresponding to a width of about 2/bandwidth is adequate under most circumstances for source signals having a Blackman shaped frequency response.

D. SEMI-COHERENT AUTOCORRELATION MATCHING

As has been done for semi-coherent localization a less coherent form of localization can be defined for the autocorrelation matching. Using Eq. 71 and Eq. 72 we can define a semi-coherent autocorrelation matching algorithm as

$$B_{RP}=\frac{\sum_{-\infty}^{\infty}|G_{RR}(\tau)||G_{PP}(\tau)|}{\sqrt{\sum_{-\infty}^{\infty}|G_{RR}(\tau)|^2\sum_{-\infty}^{\infty}|G_{PP}(\tau)|^2}}. \quad (74)$$

This form reduces the influence of the phase. Working with only positive values, however, makes the dynamic range of the ambiguity surface very small. Results for PE generated synthetic received signals and PE generated replicas look promising but the performance when comparing PE received signals and ray model replicas was not adequate to pursue this algorithm at this time.

E. THE SIFT LOCALIZATION ALGORITHM

The SIFT (Signal Integration Filtering in Time) algorithm has been developed as a result of previous research (Miller et al. 1996, Benson 1995). It is based on a ray code solution. The templates are generated using the arrival time and phase of each eigenray. These parameters determine uniquely each gridpoint in a search grid. The SIFT algorithm assumes that the signal can be written as the sum of scaled, phase and time shifted versions of the original signal, i.e.,

$$
\begin{aligned}
y(t) &= \sum_{n=1}^{N} y_n(t) \\
&= \sum_{n=1}^{N} Re(a_n \tilde{x}_p(t-\tau_n) e^{-i\theta_n}) \\
&= \sum_{n=1}^{N} a_n [x(t-\tau_n)\cos(\theta_n) + \hat{x}(t-\tau_n)\sin(\theta_n)],
\end{aligned}
\tag{75}
$$

where a_n is the real amplitude and τ_n and θ_n are the travel time and phase, respectively, of an eigenray, *x(t)* is the real source signal and $\hat{x}(t)$is its Hilbert transform. The autocorrelation of the replicas is given by

$$
\begin{aligned}
G_{yy}(\tau) &= \int_{-\infty}^{\infty} y(t) y(t+\tau) dt \\
&= \sum_{n=1}^{N} \sum_{m=1}^{N} R_{y_n y_m}(\tau).
\end{aligned}
\tag{76}
$$

The correlation between individual eigenrays can be written as

$$
G_{y_n y_m}(\tau) = \int_{-\infty}^{\infty} y_n(t) y_m(t+\tau) \tag{77}
$$

or

$$
\begin{aligned}
G_{y_n y_m}(\tau) = & a_n a_m \cos\theta_n \cos\theta_m R_{xx}(\tau+\tau_n-\tau_m) \\
& + a_n a_m \cos\theta_n \sin\theta_m R_{x\hat{x}}(\tau+\tau_n-\tau_m) \\
& + a_n a_m \sin\theta_n \cos\theta_m R_{\hat{x}x}(\tau+\tau_n-\tau_m) \\
& + a_n a_m \sin\theta_n \sin\theta_m R_{\hat{x}\hat{x}}(\tau+\tau_n-\tau_m).
\end{aligned}
\tag{78}
$$

Using properties of the Hilbert transform, this can be rewritten

$$G_{y_n y_m}(\tau)=a_n a_m G_{xx}(\tau+\tau_n-\tau_m)\cos(\theta_m-\theta_n) \\ +a_n a_m \hat{G}_{xx}(\tau+\tau_n-\tau_m)\sin(\theta_m-\theta_n), \tag{79}$$

where $\hat{G}_{xx}$ is the Hilbert transform of the real source autocorrelation, G_{xx}

In the original SIFT algorithm, three major approximations are made:

1) the amplitudes are set equal to unity (a_n=1 for all n);

2) the phases are independent of frequency;

3) the autocorrelation functions, G_{xx} and $\hat{G}_{xx}$, are approximated by discrete functions defined by

$$G_{xx}(\tau+\tau_n-\tau_m)=\begin{cases} 1 & \tau=\tau_m-\tau_n \\ 0 & otherwise \end{cases} \tag{80}$$

and

$$\hat{G}_{xx}(\tau+\tau_n-\tau_m)=\begin{cases} 1 & \tau=\tau_m-\tau_n+\delta\tau \\ -1 & \tau=\tau_m-\tau_n+\delta\tau \\ 0 & otherwise \end{cases} \tag{81}$$

where δt is chosen to be the correlation time of the measured signal.

The matching part of the algorithm is then defined by

$$S=\frac{\underline{G}_{PP}^{T}\underline{G}_{RR}}{\sqrt{\|\underline{G}_{PP}\|^{2}\|\underline{G}_{RR}\|^{2}}}, \tag{82}$$

where $\underline{R}_{TT}$ and $\underline{R}_{RR}$ are the vectors of the sampled correlations of the replicas and the received signal

$$\underline{G}_{PP}=\begin{bmatrix} -a_1a_2\sin(\theta_1-\theta_2) \\ a_1a_2\cos(\theta_1-\theta_2) \\ a_1a_2\sin(\theta_1-\theta_2) \\ -a_1a_3\sin(\theta_1-\theta_3) \\ a_1a_3\cos(\theta_1-\theta_3) \\ a_1a_3\sin(\theta_1-\theta_3) \\ \vdots \end{bmatrix} \tag{83}$$

and

$$\underline{G}_{RR}=\begin{bmatrix} G_{RR}(\tau_1-\tau_2-\delta\tau) \\ G_{RR}(\tau_1-\tau_2) \\ G_{RR}(\tau_1-\tau_2+\delta\tau) \\ G_{RR}(\tau_1-\tau_3-\delta\tau) \\ G_{RR}(\tau_1-\tau_3) \\ G_{RR}(\tau_1-\tau_3+\delta\tau) \\ \vdots \end{bmatrix} . \tag{84}$$

Usually the autocorrelation of the received signals will be formed as a linear correlation and will then be sampled. The above description assumes the eigenrays are sorted in order of increasing travel time.

A similar derivation can be made for the representation of a complex signal. The ray arrival structure can then be represented by

$$\begin{aligned}\tilde{y}(t) &= \sum_{n=1}^{N} \tilde{y}_n(t) \\ &= \sum_{n=1}^{N} a_n[\tilde{x}(t-\tau_n)e^{-i2\pi f_c\tau_n - i\theta_n}] \\ &= \sum_{n=1}^{N} a_n[\tilde{x}(t-\tau_n)\cos(2\pi f_c\tau_n+\theta_n) - i\tilde{x}(t-\tau_n)\sin(2\pi f_c\tau_n+\theta_n)\end{aligned} \tag{85}$$

In general, we may want to use signals that have been basebanded or shifted in frequency by some amount f_c. The complex source may then be defined by replacing

$$\tilde{x}(t-\tau) \Rightarrow \tilde{x}(t-\tau)e^{-i2\pi f_c\tau}. \tag{86}$$

The autocorrelation of the received signal can now be expressed as

$$\begin{aligned}G_{\tilde{y}} &= \int_{-\infty}^{\infty} \tilde{y}(t)\tilde{y}^*(t+\tau) \\ &= \sum_{n=1}^{N}\sum_{m=1}^{N} G_{\tilde{y}_n\tilde{y}_n}(\tau).\end{aligned} \tag{87}$$

To simplify the expression we define

$$\phi_k = 2\pi f_c \tau_k + \theta_k \tag{88}$$

and then the correlation between the signals of the individual eigenrays can be expanded as

$$\begin{aligned} G_{\tilde{y}_n\tilde{y}_m}(\tau) &= \int_{-\infty}^{\infty} \tilde{y}_n(t)\tilde{y}_m^*(t+\tau)dt \\ &= a_n a_m \cos(\phi_n)\cos(\phi_m) R_{\tilde{x}\tilde{x}}(\tau+\tau_n-\tau_m) \\ &- a_n a_m i\cos(\phi_n)\sin(\phi_m) R_{\tilde{x}\tilde{x}}(\tau+\tau_n-\tau_m) \\ &+ a_n a_m i\sin(\phi_n)\cos(\phi_m) R_{\tilde{x}\tilde{x}}(\tau+\tau_n-\tau_m) \\ &+ a_n a_m \sin(\phi_n)\sin(\phi_m) R_{\tilde{x}\tilde{x}}(\tau+\tau_n-\tau_m) \end{aligned} \tag{89}$$

or

$$\begin{aligned} G_{\tilde{y}_n\tilde{y}_m}(\tau) &= a_n a_m G_{\tilde{x}\tilde{x}}(\tau+\tau_n-\tau_m)[\cos(\phi_m-\phi_n) - i\sin(\phi_m-\phi_n)] \\ &= a_n a_m G_{\tilde{x}\tilde{x}}(\tau+\tau_n-\tau_m)[\cos(2\pi f_c(\tau_m-\tau_n)+\theta_m-\theta_n) \\ &\qquad -i\sin(2\pi f_c(\tau_m-\tau_n)+\theta_m-\theta_n)]. \end{aligned} \tag{90}$$

If we would apply similar approximations as with the original SIFT algorithm we would approximate the amplitude with unity and the autocorrelation function would have to be sampled with a single point approximation for $\tau=\tau_m-\tau_n$. When taking only the positive or only the negative lags into account for the approximation, the matching function would be

$$S = Re\left(\frac{\underline{G}_{PP}^H \underline{G}_{RR}}{\sqrt{\|\underline{G}_{PP}\|^2 \|\underline{G}_{RR}\|^2}} \right). \tag{91}$$

When both the negative and positive lags are used the result will obviously be real. For bandpass signals this seems a worthwhile approach. An alternative approach to accommodate bandpass signals would be to shift them to the lowest possible frequency band, form the real autocorrelation of the received signal and then apply the original SIFT algorithm for real signals.

F. SIFT AND THE PHYSICS OF THE LOCALIZATION PROBLEM

The choice of δt is one of the major difficulties with the SIFT algorithm. One way to optimize the algorithm would be to try and optimize the results for a small range of δt's. For simulations δt can easily be calculated from the cross correlation of $x(t)$ and $\hat{x}(t)$. The performance may be enhanced by optimizing over a small range of δt's, although this reduces the computational speed. For this approach to be valid, it is also necessary that δt is less than the separation between distinct arrivals and greater than the time sampling rate. For very broadband signals with good time resolution, this approximation may be very good. However, this method is quite crude and may not work for narrow band signals. An alternative may be to use a multi-point approximation instead of a three-point approximation.

The 3-point approximation of the correlation is a low frequency approximation. At high frequencies and for bandpass signals this approximation is no longer valid. Furthermore the values with which the approximation is made (1,-1,1) are dependent on the shape of the

source function. It may be worthwhile to look at a less rigid approximation. A few test cases were examined in which the Hilbert transform of the autocorrelation was neglected and no serious degradation in performance was observed.

The phase is one of the most sensitive parameters used in the algorithm. Small changes in phase at turning points and boundary interactions give the phase at larger distances a more or less random value. Although arrival structures may look similar, the autocorrelation will be very different, and much of the match is lost. For the complex envelope version of SIFT the result not only depends on the phase difference due to reflections and refractions but also on the phase difference due to the time delay. Although the travel times are known to be a very robust physical parameter in these cases, small errors may become significant at high frequencies.

In general, the calculation of eigenray amplitudes is reasonably accurate. However there are a few arrivals in those environments where the estimation of amplitudes is quite poor. Typically, these rays correspond to refracting rays near caustics producing erroneously large amplitudes. A large arrival will dominate the autocorrelation and make it look very much like the arrival structure. This may be a good reason to normalize the amplitude. When you normalize the amplitude, the later arrivals have the same weight in the correlation and, therefore, in the matching algorithm as the earlier arrivals. This has a number of advantages. The later arrivals carry as much information as the first few and, therefore, taking them into account increases the amount of information in your match. Also solutions of the eigenray extraction routine are more stable for the later arrivals than for earlier arrivals.

IV. EXPERIMENTAL SETUP AND RESULTS

To gain insight into the performance of the autocorrelation matching algorithms and approximate autocorrelation matching algorithms, several computer experiments have been done. The experiments have primarily been performed for a frequency band of 750-1000 Hz. The baseline for the results was defined as the results of the autocorrelation matching of a PE generated source and PE generated templates. For most of the experiments a source range of 5500 m, a source depth of 59.8 m and a receiver depth of 40.2 m have been assumed. For the environments defined below, at this range the first arrivals arrive at approximately 3.7 seconds after the transmission and the significant part of the arrival structure is about 0.4 seconds in length. As the project did not focus on the frequency characteristics of the source function, the same shape has been assumed for the source signal and the templates. Throughout the project analysis the absolute scale of the pressure field calculation has been neglected as the similarity of the arrival structures is emphasized not the absolute values of the pressure field.

A. ENVIRONMENTS

For the synthetic experiments, three shallow water, range independent environments have been defined. The first has a negative sound speed gradient (1500-1475 m/s), the second has a constant sound speed of 1500 m/s, while the third has a positive sound speed

gradient (1500-1501.5 m/s). All other acoustic parameters are fixed for the three environments. The water depth is 100 m and the bottom parameters, the attenuation, density and sound speed, were chosen as α=0.48 dB/(km Hz), ρ_{bottom}=1900 kg/m^3, c_{bottom}=1650 m/s, respectively, consistent with a sand bottom. The bottom is modeled as an infinite half space in both propagation models. The propagation loss for the environments at a frequency of 875 Hz is shown in Fig. 3 (a), (b), and (c). These plots suggest a very rapid variation of the acoustic pressure with respect to depth. The vertical size of localization footprints is therefore anticipated to be small.

The third, positive gradient, environment has only been used to generate a limited set of ACM baseline results. It was, perhaps wrongly, anticipated that the results might not significantly differ from the results generated for the iso-speed environment, and therefore the computational effort would not outweigh the additional results. While this appeared to be the case for the third environment (with a weak positive gradient), the results for the first environment (strong negative gradient) were significantly different. The analysis suggested that most of the algorithms performed well for the second environment (iso-speed) but were at their performance limits for the first environment. It is therefore likely that a less severe sound speed gradient environment could have given more insight into the exact performance limits of the algorithms.

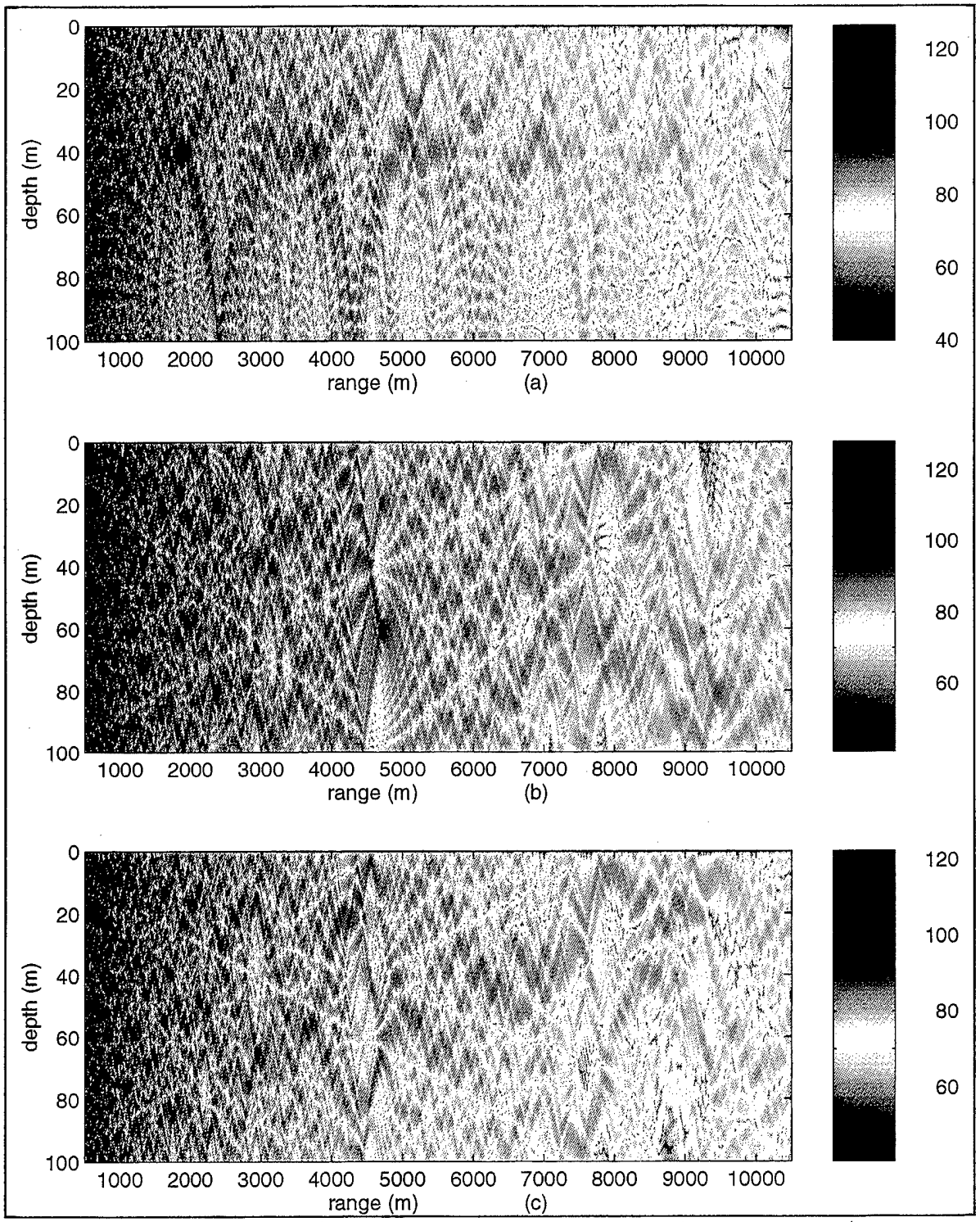

Figure 3 Transmission loss at 875 Hz for (a) a negative sound speed gradient (1500-1475 m/s) environment, (b) an iso-speed (1500 m/s) environment, and (c) a positive sound speed gradient (1500-1501.5 m/s) environment.

B. HAMILTONIAN RAYTRACING PROGRAM FOR THE OCEAN

The Hamiltonian Raytracing Program for the Ocean (HARPO) has a number of parameters which directly influence the accuracy of the results. To be able to use the results for this application, a maximum ray launch angle separation of 0.05 degrees has been determined. Larger spread caused unacceptable inaccuracies in the eigenray extraction program. The program has been set to output all the points, and the integration accuracy has been set to 10^{-6}. Less accurate settings would degrade the performance of the eigenray extraction program. Travel times and eigenray calculations have been compared with results from an analytical model and proved to be very accurate. To reduce the computational burden, the assumption has been made that at the ranges of interest the attenuation due to bottom reflections would be high enough such that source angles larger than critical could be neglected. This reduces the number of eigenrays to about 40-50 per grid point for the negative gradient environment for a range of about 5 km. For shorter ranges, source angle limits of ±40 degrees have been used resulting in more than 18 eigenrays per grid point for ranges above 1 km. This set up resulted in a ratio of the smallest to the largest eigenray amplitude per grid point of smaller than 0.02 for 95% of the environment. The grid point spacing of the eigenray extraction routine has been set to 5 m in range and 1.4 m in depth. The depth spacing does not meet the initial minimum requirement of five grid points per

dimension of the footprint (12.5 m x 1.2 m at 5.5 km for a source depth of 59.8 m and a receiver depth of 40.2 m). It is a compromise due to the computational speed of the eigenrays extraction routine.

During the experiments, four eigenray extraction problem areas were indicated. Very abrupt change, or little change, together with noise due to round off and interpolation errors and using too large angle separations creates either too few or too many eigenrays or 'spurious' eigenrays at these points. For the iso-velocity environment, a separate program has been used that is based on an analytical solution. This allowed a little more flexibility and considerably reduced the run time.

C. UNIVERSITY OF MIAMI PARABOLIC EQUATION MODEL

The University of Miami Parabolic Equation Model (UMPE) was used with the wide-angle PE approximation, as described in Chap. II. The maximum computational depth has been set to 409.60 m. A depth spacing of 40 cm leads to 250 grid points within the water column, and 4-5 grid points per wavelength. As a comparison, only 70 grid points in depth have been used to cover the water column for the ray model. The grid spacing in range has been set to 50 cm which is about the minimum for an accurate prediction in the environments described above. Results have been stored in 2.5 m and 5 m range increments for the negative gradient and iso-speed/positive gradient environments, repectively. The frequency is sampled from 750 Hz to 1000 Hz in 257 frequency bins. At a range of 6500 m,

this frequency resolution still allows the calculation of the correlation as the Fourier transform of the power spectral density without degradation due to wrap-around.

D. RECIPROCITY

In the experiments, the source and receiver are assumed to be a point source and a point receiver. The source spectrum is shaped as a Blackman window. This avoids large sidelobes in the time domain arrival structure and leads to a pulse length of approximately 8 ms. To optimize the eigenray extraction routines, a large number of reciprocity checks for different source and receiver locations have been done. The autocorrelation function of the arrival structures proved to be an excellent tool in cases where the arrival structures looked alike. Small differences in amplitude and especially phase led to large differences in the autocorrelation function. This suggested that localization algorithms based on the time domain autocorrelation would be very sensitive to these parameters, particularly the phase.

The PE-results showed very good reciprocity. The ray code results showed good reciprocity except at certain locations where erroneous amplitude calculations degraded part of the arrival structure. Looking at the difference between the ray code and PE arrival structures, it appears that the largest difference can be found in the first few arrivals. The tails of the arrivals structures are very similar. This suggests that the ray code approximation for refracting rays is less accurate than for reflecting rays. Perturbation analysis of the phase and amplitude of the rays suggests that the arrival structures and autocorrelation are more

susceptible to phase errors than to amplitude errors. Results also suggest that certain parts of the autocorrelation are more affected than others. Very short lags and very long lags seem to suffer more than intermediate values. Knowing that short lag values are notched out and large lag values will have no significant contribution to the match suggests that the algorithms should at least have some degree of tolerance toward amplitude and phase errors. This suggestion is based on visual analysis of a large number of results, but no statistical analysis has been performed.

E. MATCHING ALGORITHMS

Numerical experiments have focused on autocorrelation matching and the SIFT matching algorithm. The baseline for the results has been defined by the PE autocorrelation matching over the full 250 Hz bandwidth using a Blackman shaped frequency response. The autocorrelation matching experiments can be separated into their variations of the basic algorithm. The following variations have been specifically examined: 1) the effect of notching out points near zero lag; 2) the effect of using a smaller bandwidth, which was anticipated to give a larger footprint size; 3) the effect of splitting up the frequency band into several smaller frequency bands; 4) the effect of a lower frequency resolution; 5) the effect of raising the tail of the autocorrelation function, i.e. to increase the weight of large lag values (corresponding to cross terms of early and late arrivals); 6) the effect of matching the

absolute values of the autocorrelations functions; and 7) the effect of amplitude and phase perturbations on the frequency domain arrival structure.

Specifically for the ray results, additional effects have been examined: 1) the effect of raising the tail of the arrival structure to increase to weight of the later arrivals; 2) the effect of neglecting the first few arrivals, as the amplitude and phase of these arrivals are suspected to be the cause of most of the bad results; and 3) the effect of matching the arrival structures directly, in both complex and absolute form.

The SIFT algorithm has been considered in four different ways: 1) a form where the complex signals have been base-banded and a 1-point approximation to the autocorrelation function is used; 2) a form where the real signals are shifted in frequency to a center frequency of half the bandwidth and where subsequently a modified form of the original SIFT algorithm is employed; 3) a form where the signals are shifted and then a zero mean version of the original SIFT algorithm is employed which results in a multiple-point match; 4) variations on the original low frequency implementation of the SIFT algorithm. For all the variations, notching out points near zero lag, neglecting early arrivals, and variations of the parameters that describe the approximation to the correlation functions applied in SIFT have been considered.

The grid spacing of the templates has been based on the footprint size of the baseline results and computational arguments. As the main area of interest is beyond 5 km, the results of autocorrelation matching at 5.5 km for the negative gradient environment have been used for determining the footprint. The footprint size is approximately 1.2 m in depth and 12.5

m in range. With a norm of 5 points per dimension of the footprint this would lead to a grid spacing of 20 cm in depth and 2 m in range. Analysis at other ranges suggests the footprint will be smaller at smaller ranges and larger at larger ranges. The excessive run time of the eigenray extraction, the available disc storage and run time for the matching algorithms have lead to a grid spacing of 2.5 m in range and 40 cm in depth for PE generated templates in the negative gradient environment, 5 m in range and 0.4 m in depth for PE generated templates in the iso-speed and positive gradient environments, and 5 m in range and 1.4 m in depth for the ray code generated templates. For the negative gradient environment, the eigenray results have only been calculated for 1000-2000 m and 4500-6500 m due to the computational load of the MATLAB based eigenray extraction routines. Attempts to apply the recently available MATLAB c-compiler were not successful. The presently available compiler still uses many standard MATLAB routines which prevent generation of efficient code. Also the nature of the problem which relies on using complex numbers degrades the ability to generate efficient code.

To generate synthetic 'received' signals, three basic algorithms have been used: an impulse model based on Eq. 43, a time domain model based on Eq. 33, and a frequency domain model based on Eq. 37. Where the impulse model is an inherently low frequency model, the time domain model is suited primarily for band pass signals. A small modification to the original time domain based model developed by Chiu made it suitable

for low frequency applications. In the time domain model, the tails of the pulse are removed which is a major advantage in testing algorithms where overlap of pulses is a crucial parameter.

The autocorrelation of the synthetically generated received signals has been computed using several different methods. For autocorrelation matching using frequency based data as generated by the UMPE model, it may seem that the transform of the power spectral density may be the most practical solution. However the circular convolution does not work well with pulse signals where the pulse length is more than half the transform time base. For this reason the autocorrelation for this project has primarily been computed from the time domain arrival structure. Where in previous work an 'unbiased' autocorrelation estimate has been used, for this work the 'biased' autocorrelation estimate has been used which is more suited for pulse shaped signals. As the time base is determined by the frequency resolution, it may be beneficial in future experiments to artificially stretch the time base before performing the autocorrelation. Results of applying phase disturbances to the PE results suggested that keeping the time domain arrival structure centered in the first half of the time base can not always be accomplished. While theoretically PE phase errors should have no influence on the autocorrelation results, there will be a degradation in the results due to the above. Thus, while theoretically the time domain based autocorrelation may be preferable, in practice the frequency domain based calculations are more robust.

No use has been made of the usual performance measures such as peak to sidelobe level or mismatch in range and depth. The reason is that these measures tend to put a

number to a match. This work tries to explain how and why the match will degrade. It has been observed that a match tends to become amplified along certain lines of high correlation/energy. Furthermore, when the matching parameters exceed certain values, depending on the type of matching, environment, range and bandwidth, the results suggest the single match will explode into several 'matches' spread around the actual source location. This still gives an indication of the source location but it will not give a single point match.

F. COHERENT MATCHING RESULTS

Coherent matching has been performed in the time domain and in the frequency domain. The frequency domain approach may require an additional parameter to allow for time shifts. All presented analysis uses a time domain approach. Results may slightly differ due to the time resolution used. Results for the negative gradient environment with a source at 5500 m display sidelobe levels comparable to autocorrelation matching with an optimum number of lag values notched out. The footprint size for the same setup was found to be larger for the coherent matching than for the autocorrelation matching. Coherent matching results using ray code templates and PE generated source signals showed some phase shift between the templates and the source signals. In general, we were able to localize correctly up to ranges of more than 5 km. Short ranges resulted in very high sidelobes, especially in the iso-speed environment. No significant changes have been made to the basic coherent matching algorithm. In many cases where the autocorrelation matching algorithms failed to

localize, the coherent matching still gave reasonable results. Taking into account a phase shift in the result of the match improved the performance significantly. There are however many drawbacks to coherent matching, and there are locations where we found that many templates and the received signal were almost alike which led to very high sidelobes. Discretized phases may be a convenient way to improve the coherent matching algorithm.

In addition some analysis has been done on a less coherent approach using the absolute value of the time domain arrival structure. The dynamic range was improved by subtracting the average over a certain area of the matching resuls. Altough baseline results showed promising, the results using PE generated received signals and ray code generated templates showed very high sidelobes which prohibited correct localization. A similar approach will be discussed further in Chapter V.

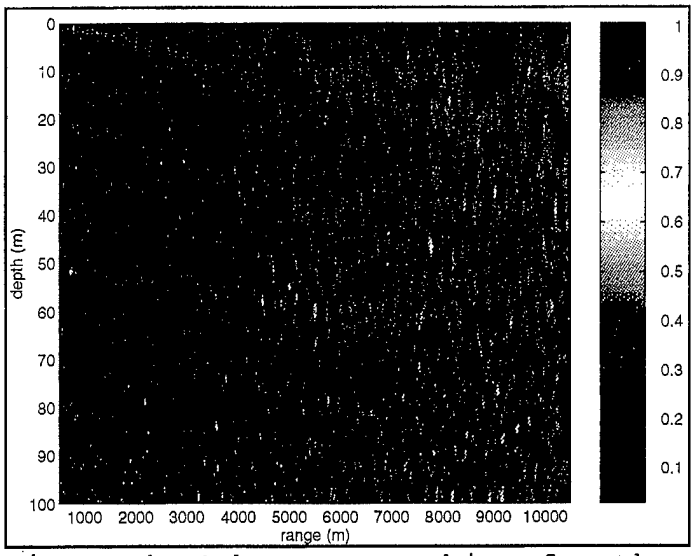

Figure 4 Coherent matching for the negative gradient environment (baseline result), with a source at 5500 m range and 59.8 m depth and a receiver at 40.2 m depth.

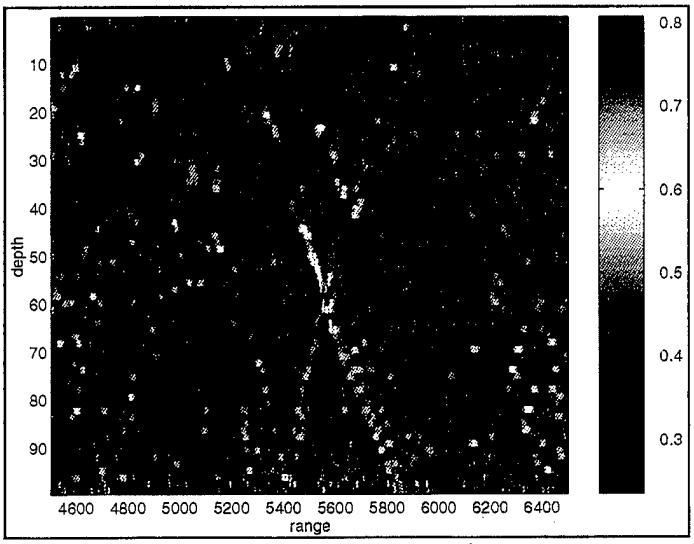

Figure 5 Coherent matching for the negative gradient environment using a PE generated source signal and ray code templates with a source at 5500 m range and 59.8 m depth and a receiver at 40.2 m depth. Accounting for the phase shift results in correct localization.

G. AUTOCORRELATION MATCHING RESULTS (BASELINE)

The autocorrelation matching algorithm is described in Chap. III, Section C. To improve upon the results of the basic algorithm, the following variations have been considered: notching out near zero lag values; enhancing the dynamic range by subtracting the average over a certain area of the match and renormalizing; increasing the significance of large lage value by filtering; changing the sample rate, bandwidth and frequency resolution; and splitting the frequency band into several small bands. To get an initial assessment of the robustness, amplitude and phase perturbations have been added to the PE generated received signals and PE generated templates.

Results for both the negative and positive gradient environments and a source at 5500 m range suggest that notching out zero lag and the first 2-4 lag values (corresponding to (1 or 2)/BW) gives an optimal performance in terms of peak to sidelobe level. For the isospeed environment the optimum was found by notching out four times the previous number of lag values, having still larger sidelobes than the other two environments. Presumably arrival structures are more similar for the iso-speed environment. Results suggest that the optimum number of notched out lag values depends on range and, to a lesser extent, on bandwidth (except for low frequencies where the bandwidth dominates). The first few lag samples represent the low frequency trends in the autocorrelation. They are more related to the power in the signal rather than the shape and will dominate the match when they are not removed. Notching out these lag values, however, decreases the footprint size.

Notching out more than the optimum number of lags does not significantly reduce the footprint size any further for the negative gradient environment. For the iso-speed environment, however, the footprint size continues to decrease further when the number of notched out lag values increases.

As an alternative to notching out values around zero lag in the time domain, two approaches have been considered. Removing the mean from the frequency domain results leads to similar results as notching out only the zero lag value. Removing lower order trends would require filtering of the power spectrum, which makes it much more complicated than notching out values in the time domain, with theoretically the same results. The second approach aims to increase the dynamic range, and is based on the subtraction of the matching value, averaged over an area, from the individual matching values. Contrary to notching out values around zero lag, this approach has no real physical interpretation. The results are comparable. However sidelobe levels are slightly higher, and it does not have the degrees of freedom to optimize the results as with notching out lag values in the time domain.

The footprint was found to depend on range, receiver/source depth, sound speed profile, position of the source relative to the 'lines of high correlation/energy', and on bandwidth. It was found for the cases considered that the general trend is for the footprint to increase with range. Footprints for the same source/receiver depth were found to be much larger than for significantly separated source receiver depths. In general, footprints tended to be larger for the environment with a small positive gradient and the iso-speed

environment than for the environment with a large negative gradient. The position relative to a line of high correlation/energy determines if and how the footprint will stretch. The most significant difference between the slight positive gradient or iso-speed environment on one hand and the severe negative gradient environment on the other is the vertical extent of the footprint which is nearly twice as large for the slight positive gradient and even larger for the iso-speed environment than for the negative gradient case. The smaller footprints of the negative gradient environment can be directly related to the more severe interference patterns. The significantly larger footprints for the same source receiver depth are thought to be caused more by energy matching than by matching of the arrival structure shape.

The number of points or sample rate did not appear to be a crucial parameter. There are some results suggest that a sample rate of 1000 Hz might give better results and a slightly larger footprint than a sample rate of 250 Hz. For this reason the bulk of the analysis has been performed for a sample rate of 250 Hz for the negative gradient environment and 1000 Hz sample rate for the iso-speed environment. Contrary to our initial expectations, smaller bandwidths generally produced smaller footprints and higher sidelobes than larger bandwidths. This may be due to fewer arrivals being sampled at smaller bandwidths cause the the autocorrelation (and its match) to drop off rapidly away from the source location. Larger bandwidths on the other hand, resolve more multipath arrivals which may broaden the autocorrelation and generate a larger footprint.

A lower frequency resolution showed a larger footprint but also large sidelobe levels. Although the number of cases examined is limited, the results suggest that larger bandwidths are preferable, as expected. Results also suggest that it may not be necessary to apply any window. Results show that the degradation due to sidelobes/ringing in the time domain may be outweighed by the increase in performance due to the larger bandwidth.

Separating the 750-1000 Hz band into 4 smaller bands and averaging the results led to a slightly larger footprint as compared to the full bandwidth results but with a significant increase in sidelobe levels. Later arrivals are more separated in time than earlier arrivals and are also more stable in these environments as they are not related to refracted propagation paths. To be able to exploit them, the later arrivals should be enhanced. In the PE model the individual arrivals cannot be manipulated. Therefore, an alternative approach was used, enhancing the tail of the autocorrelation. Results suggest that indeed some improvement may be gained with this approach in terms of the sidelobe levels, especially if it is applied to both the received signals and the templates. The footprint, however, appears to be smaller than for the full bandwidth case (7.5 m in range and 2.5 m in diameter at 5.5 km for the negative gradient environment). The results were not found to be significant enough to pursue this approach any further. It may be that in more complicated environments this approach should be reconsidered.

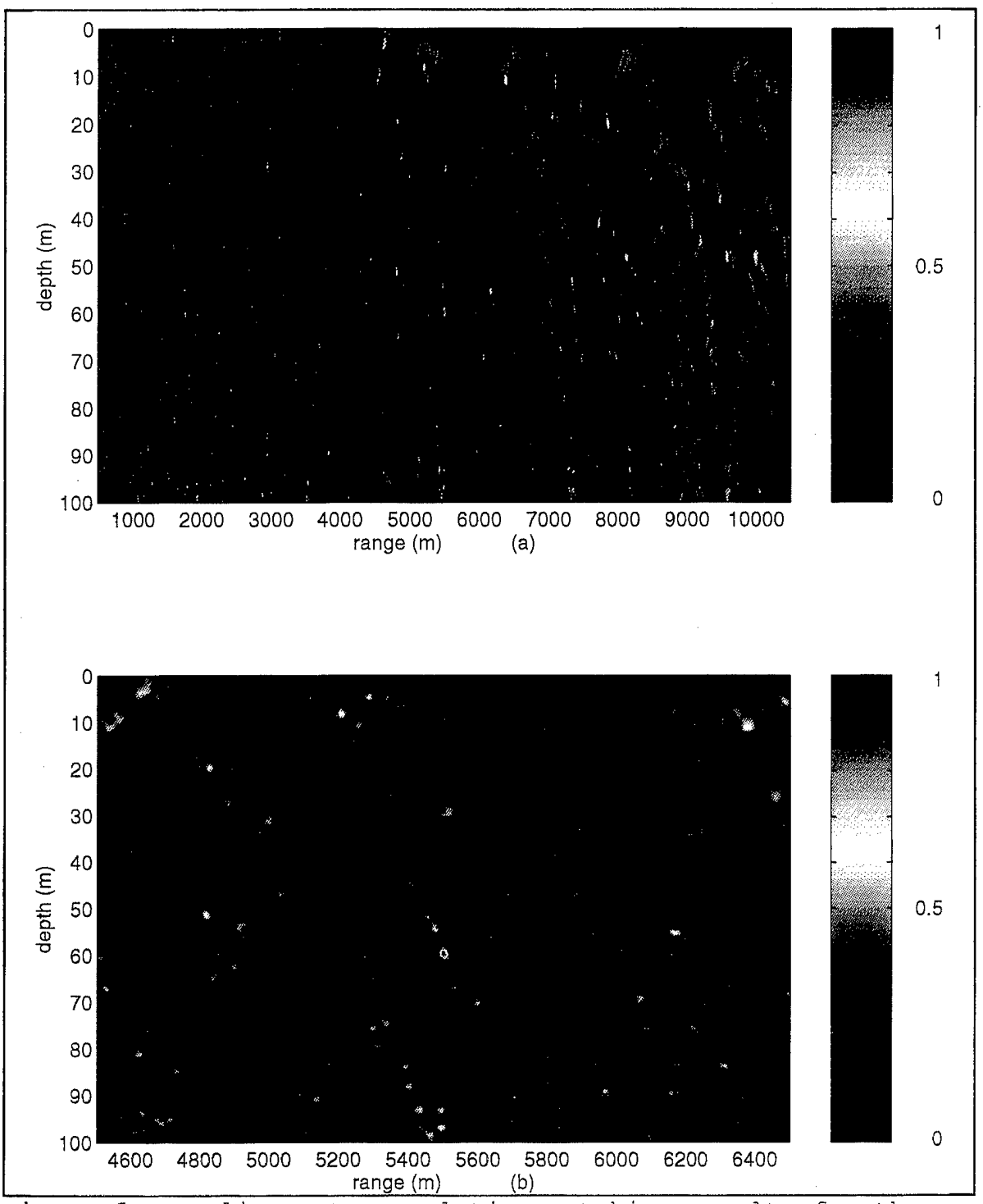

Figure 6 Baseline autocorrelation matching results for the negative gradient environment. The source is located at 5500 m range and 59.8 m depth and the receiver at 40.2 m depth. Three notched out near zero lag values have been used. (a) Full range. (b) Range expanded near the source location.

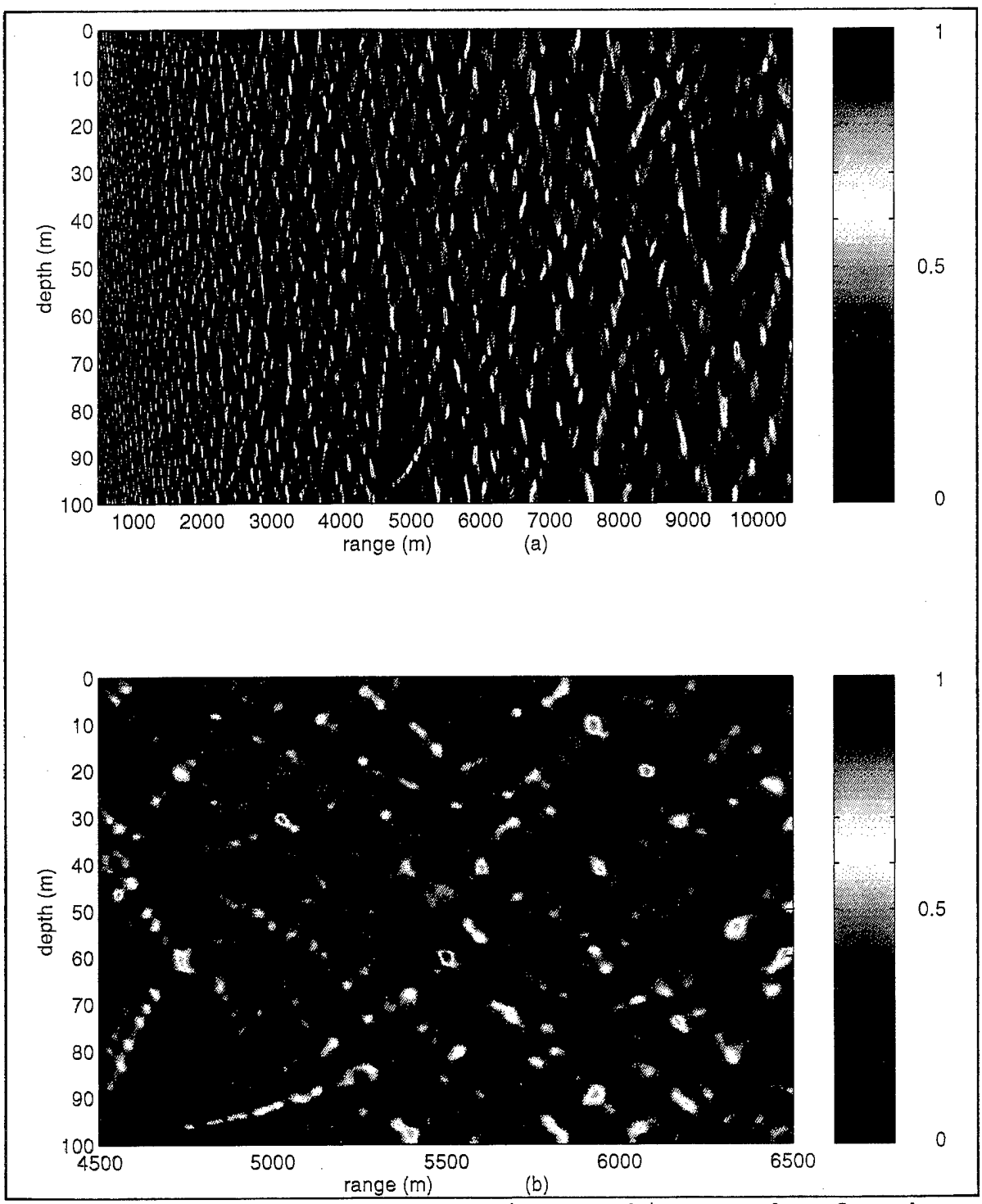

Figure 7 Baseline autocorrelation matching results for the iso-speed environment. The source is located at 5500 m range and 59.8 m depth and the receiver at 40.2 m depth. Three notched out near zero lag values have been used. (a) Full range. (b) Range expanded near the source location.

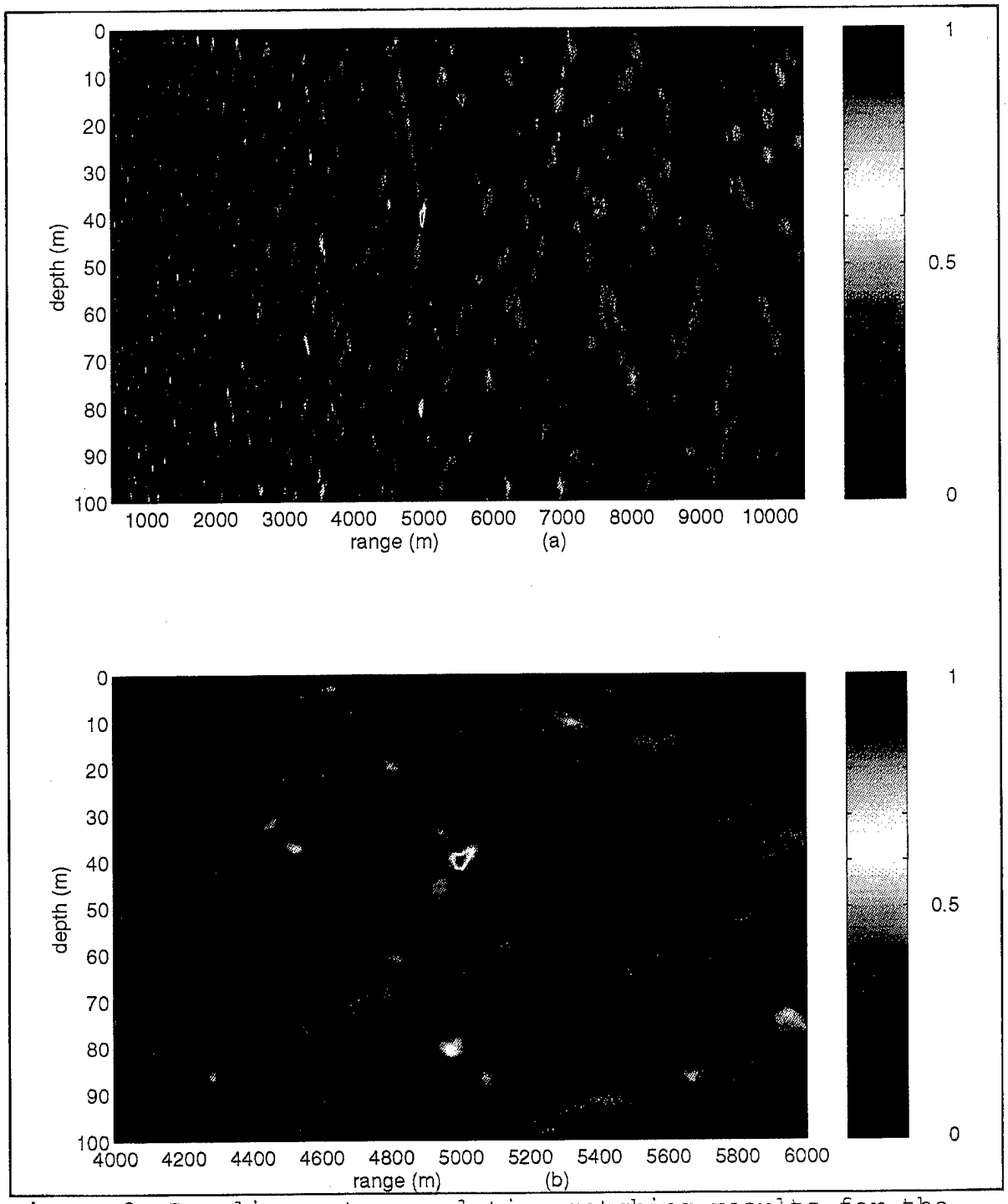

Figure 8 Baseline autocorrelation matching results for the positive sound speed gradient environment. The source is located at 5000 m range and 40.2 m depth and the receiver at 59.8 m depth. No window has been applied and 3 near zero lag values have been notched. (a) Full range. (b) Range expanded near the source location.

To get an assessment of the robustness of the algorithms amplitude and phase perturbations have been applied. The effect of phase perturbations has already been discussed. The amplitude perturbation has been applied as a uniform random fluctuation. Using a random distributed amplitude fluctuation up to +/- 40 % only showed a reduction in the peak to sidelobe level, but no significant increase in sidelobe levels or change in the footprint size were observed. This indicated that the algorithm is fairly robust for amplitude fluctuations.

H. AUTOCORRELATION MATCHING (NUMERICAL RESULTS)

When matching PE source signals and ray code templates for the negative gradient environment using a windowed frequency response, results appear to be changing periodically for ranges beyond about 5 km. Moving the source over a range increment of 4500-6500 m, a correct localization was obtained about 50% of the time. Of the remaining half, some regions, did not show any localization while in other places the localization was obscured by high sidelobes. Short ranges give more consistent results but also contain inherently high sidelobes. Even with a severely inadequate ray set, localization could be performed at ranges up to 2000 m.

Several changes have been made to obtain more consistent results at longer ranges. Notching out a large number of lag values sometimes improves the results but not consistently. Applying a window that amplifies the larger lag values of the correlation gave some improvement when applied to both the received signal and the templates.

From the good localizations, a 1.2% difference in range between the ray code solution and the PE solution was found for the negative gradient environment. This difference is probably due to phase errors in the PE approximation or a sub-optimal choice for the reference sound speed and using below optimal values for the range and depth grid spacing. The footprint size is usually very small, 5-15 m in range and 1.4 m (1 grid point) in depth. Neglecting the initial arrivals in the ray code solution did not improve the results. It also seems that higher sampling rates give slightly higher matching peak values but do not significantly improve the results. Splitting the frequency band into several smaller bands can improve the results for a certain set of matching parameters, but the results are not predictable. No solid reason could be found explaining the changing behavior with range. It is speculated that this is not directly related to the bandwidth (smaller bandwidths sometimes produced better results than larger bandwidths) but may be related to the modal interference pattern, the phase errors in the initial arrivals, and possibly under-sampling.

No correlation was found between eigenray amplitude problem areas, eigenray extraction problem areas, arrival times, arrival time differences, depth of the perigee of refracted rays, or number of refracted rays and the changing behavior with range. The phase of the 'half' match (using only positive or negative lag values) was observed to vary

periodically. But as it is composed of many parts, it is more indicative than a real measure, and it shows no sudden changes for locations where a match was expected but not found. A fixed phase difference in the time domain should not show in the autocorrelation. Still, as other methods do not seem to suffer as much, the reason is presumably related to the autocorrelation.

The only link to an explanation may be found from results which were obtained without a frequency window. Using the full 250 Hz bandwidth without frequency windowing led to correct localizations where no localization was found with windowing. This suggests that any degradation due to sidelobes of the window function is outweighed by the improvement due to the effective larger bandwidth. An additional improvement was achieved by accounting for the phase shift in the 'half match', which led to a considerable enhancement of the peak to sidelobe ratio. These results may also suggest that the required bandwidth is not a monotone increasing function of range and the sound speed profile probably has a distinct influence on that relationship.

For the iso-speed environment, good localization is found over the whole range from 900-7500 m. At larger ranges the performance is better than at short ranges due to the higher sidelobes at short ranges. Footprints are slightly smaller than for the baseline results. These results were not found to be very sensitive to the time sampling rate, in contrast to the baseline results.

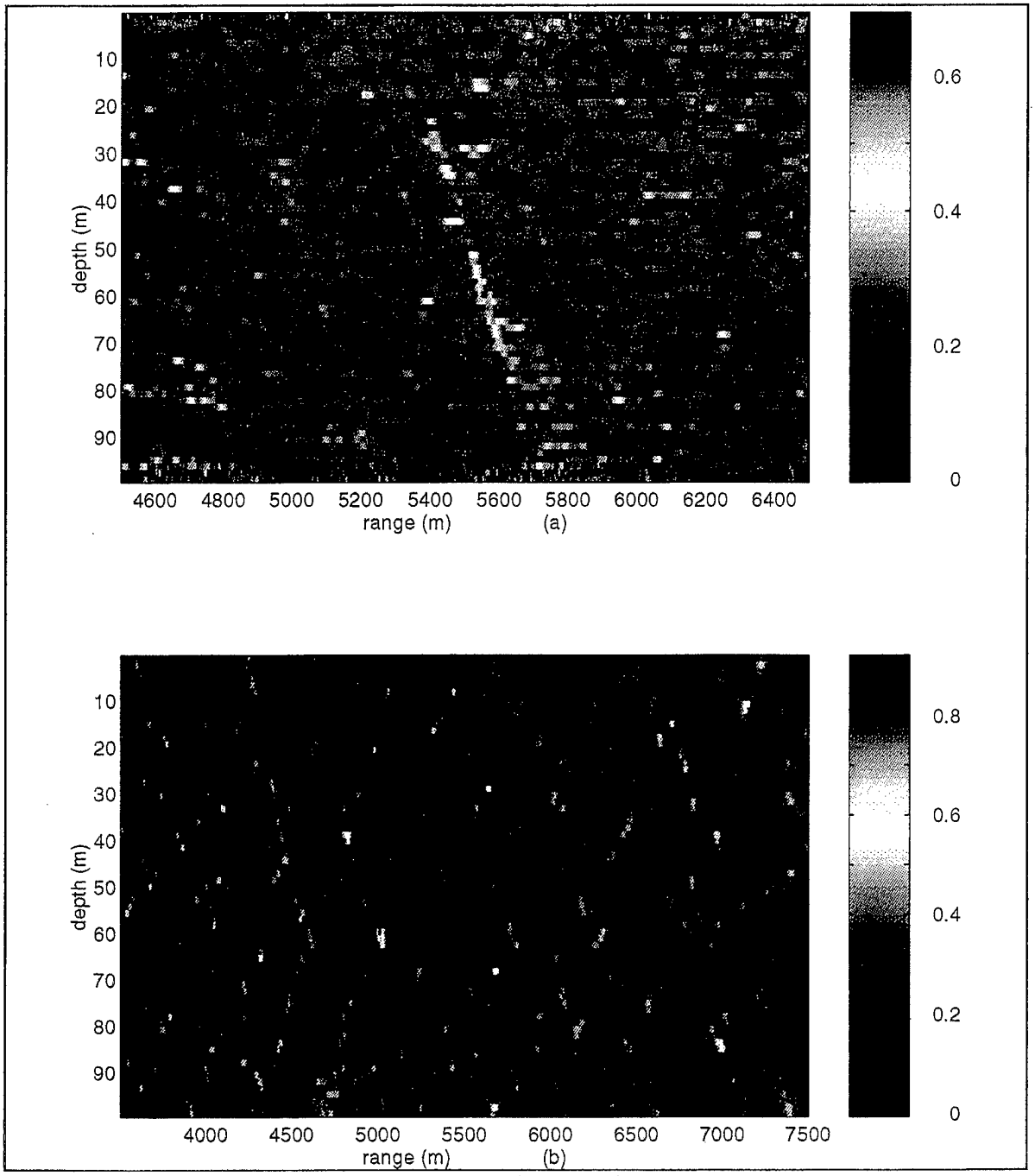

Figure 9 Autocorrelation matching using a PE generated source signal and ray code templates.(a) Negative gradient environment with a source located at 5500 m range and 59.8 m depth and a receiver at 40.2 m depth. Full 250 Hz bandwidth has been used without window and the phase difference of the autocorrelations has been accounted for.(b) Iso-speed environment with source at 5000 m range and 59.8 m depth and receiver at 40.2 m depth.

I. SIFT MATCHING RESULTS (LOW FREQUENCY)

The SIFT matching algorithm that was developed by Miller and others (Miller et al, 1995), has been modified to account for bandpass signals, to bring it closer to a true autocorrelation matching, to improve the notching for short time lags, to adapt it for 1- to n-point matching instead of the fixed 3-point matching, to manipulate the amplitude of the cross correlation of the source function and the Hilbert transform, and to include the ray amplitude in the matching. The original SIFT algorithm is based on a source signal that behaves like a low frequency pulse signal. This type of signal has been proven adequate for modeling of SUS charges. However, it may be less suitable to describe other signals, especially signals which have been high-pass filtered. For this kind of signal an n-point match, where n increases with decreasing bandwidth, may be more appropriate although the matching may become too complicated for large n. In certain favorable cases, tuning of the δt factor in Eq. 81 may even allow the use of a 3-point match when using a signal that does not resemble the assumed signal model.

The original SIFT algorithm will never give a perfect match even if the received signals can be modeled as spikes. This is because the cross correlations are stacked as an array rather than summing the cross correlation of individual arrivals, . However, this result is matched with the sampled autocorrelation of the received signal in which the individual arrivals are inherently added coherently. As this addition slows down the algorithm, it has not always been used.

The notching previously was based on the arrival time difference. It did not take into account the approximated cross correlation of two arrivals containing two points that were shifted by δt. In the algorithms used here this slight modification, which may be important at short lags, was taken into account.

Algorithms for the 3-point matching have been implemented. The n-point matching algorithm has been considered but given the time scale it was not implemented. As the source function of the received signal was known, the amplitude of the 3-point approximation of the cross correlation has been tuned to optimize the performance. For an n-point SIFT algorithm, this would be an immense task and not conducive to working with real data.

The amplitude of the rays has been brought back into the SIFT algorithms in contrast to previous versions. In general, this improved the results but only slightly. A few cases even showed a degradation of the results when ray amplitudes were included in the algorithm.

Aside from the parameters mentioned above, the following parameters were taken into consideration to optimize the results: the offset δt, the sampling rate, and the bandwidth.

To develop some intuition about the general performance, the low frequency version of the algorithm has been applied to the negative sound speed and iso-speed environments. The results imply that the performance of the algorithm for a certain environment, source function, bandwidth, and bottom depth is range limited. An empirical analysis suggests that the area where the algorithm performs succesfully is below the curve

$$d > k\sqrt{\frac{r\bar{c}}{B}}, \tag{92}$$

where d is the water depth, $\bar{c}$ is an average sound speed, B is the true bandwidth, r is the range and k is a constant that depends mainly on the environment. The constant k ranges from approximately 0.35 to approximately 0.5 for the iso-speed and negative gradient environments. The approximate curves for the iso-speed and negative gradient environments are depicted in Fig. 10. There is strong evidence that the curves describe the areas where the algorithm is likely to perform, but not enough analysis has been done to exactly localize the curves. The formula is based on a first order approximation of the arrival time differences for r>>d.

Results suggest that there may be different regimes which govern the matching. First, there are the high bandwidth cases which are well below the curve described by the parameters. It is suggested that the match consists of different contributions, most probably energy and shape of the arrival structure, which are influenced by the number of notched out values. For high bandwidths, the shape of the arrival structure prevails. When the bandwidth is reduced, the shape of the match stretches along the lines of high correlation/energy (most probably corresponding to rays with dominating amplitudes). Reducing the bandwidth further causes the match to split up into several 'matching points' which migrate along the lines of high correlation/energy. The improvements mentioned earlier give some relief but

only marginally increase the performance. Plots of the number of sampled cross correlations with lag values within one pulse width do not show any abrupt changes with decrease in bandwidth.

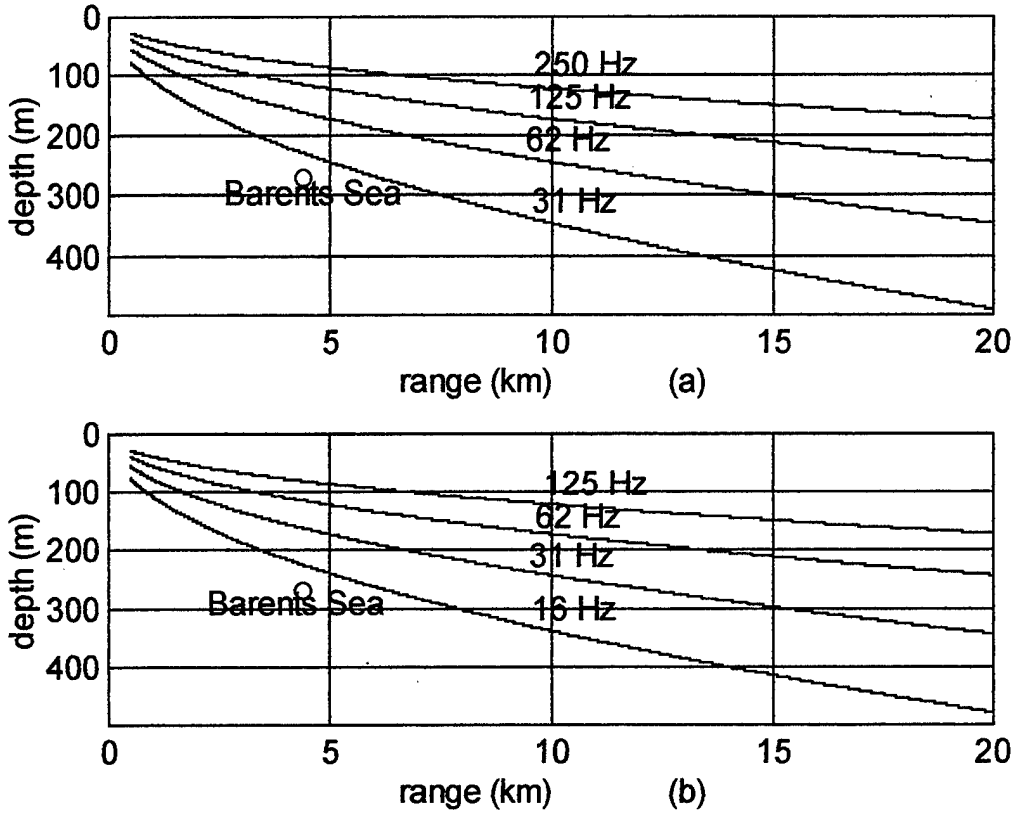

Figure 10 Estimated performance limitations for the LF SIFT algoritm for (a) the negative gradient environment and (b) the iso-speed environment.

The autocorrelation of the received signal however gives a clue to the process. During the reduction of the bandwidth, a low frequency trend starts to dominate the arrival structure of the received signal. The individual arrivals seem to ride on top of this low

frequency trend. In the autocorrelation, the sequence of the positive/negative going parts of the arrival structure becomes dominant. This makes it necessary to notch out about twice the number of points notched out at higher bandwidths. At these low bandwidths, performance is not impressive and the footprints are large and only approximate localization is possible, but the sidelobes are excessively large. It is still unclear whether we could exploit this last regime, especially in more complicated or more noisy environments. The change in the autocorrelation of the received signal indicates the limit up to where the algorithm can be pushed in the ordinary form. Results for both environments considered differ but the trend agrees with the theory. As the significant arrivals for the negative gradient environment are more confined in time than for the iso-speed environment, the limits for a certain algorithm in this environment are more severe. No low frequency synthetic PE source signals have been used because results of the ray model and UMPE model are largely different below 10 Hz due to the breakdown of ray theory at these frequencies.

The size of the footprint is found to be dependant on range and bandwidth. In general, a larger bandwidth will give a smaller footprint. The numerical analysis presented here indicated that a bandwidth of 250 Hz at a range of 5 and 7.5 km was not adequate for the algorithm to succesfully localize for the negative sound speed gradient environment. Consequently, some of the goals of the project based on these parameters had to be dropped.

Results show only moderate sensitivity to the offset parameter δt, and in some cases a forced 1-point match (neglecting the cross correlation of the source function and its Hilbert transform) performs just as well as a 3-point match. The optimum offset parameter showed

to agree well with theory. Using the calculated amplitudes in SIFT instead of setting them to unity generally improves the results except when the amplitudes are totally in error. Thus, with amplitude variability being a major issue in real data, this approximation may be validated, in general.

To be able to explain the good performance of the algorithm in the Barents Sea experiments, we note that the location of the experiment was more than 250 m deep, the signals were essentially low frequency, and the low frequency variant of the algorithms was used. The bottom was modeled as a hard bottom and attenuation was modeled as rough surface scattering, a reasonable approximation for this area. Both synthetic and real (SUS) sources were used. The source range was approximately 4.5 km, the source depth was 15 m and the receiver depth was 170 m for most of the analysis. Applying the results found in this thesis suggests that the larger depth was a crucial point in the performance of the algorithm in the Barents Sea analysis. In addition, shallow source depth and large grid spacing in range cause any change in the shape of the matching point to be resolved in the same resolution cell.

J. SIFT MATCHING RESULTS (HIGH FREQUENCY)

Both the 1-point and 3-point high frequency SIFT matching algorithms were found not to be able to localize in the negative gradient environment beyond 4500 m. In addition, the 3-point algorithm was not be able to localize at ranges shorter than 2000 m. The 1-point

algorithm localizes correctly at ranges shorter than 2000 m but shows high sidelobes. Beyond 4500 m both algorithms show an area of high sidelobes around the actual source location. This is only seen for very high bandwidths (>250 Hz true bandwidth).

The time domain arrival structure of the received signal for the 3-point match shows a large onset corresponding to the Hilbert transform component of the main arrival. This results in an offset in the autocorrelation which may partly explain the difficulties with the algorithm. Using ray code generated source signals shows good performance for both algorithms even at 250 Hz bandwidth. This suggests that it might even be a programming error since these results should experience the same difficulties.

Both the 1-point and the 3-point algorithms show good performance for the iso-speed environment. Manipulating the individual amplitudes in the 3-point match does improve the results but only slightly. Other results, however. suggest that the add and compare approach, discussed earlier, may improve the 1-point and 3-point matching results at larger ranges. Some results suggest that both high frequency algorithms require even more bandwidth than the low frequency version of SIFT. Unfortunately, this might not be possible in practice. It is expected that there might be some better performance for the 3-point matching algorithm in the 2-4.5 km range. The more general n-point SIFT algorithm has not been used as it was expected to suffer even more from the limited bandwidth, and it was considered to be very difficult to tune the individual δt's and amplitudes of the components correctly.

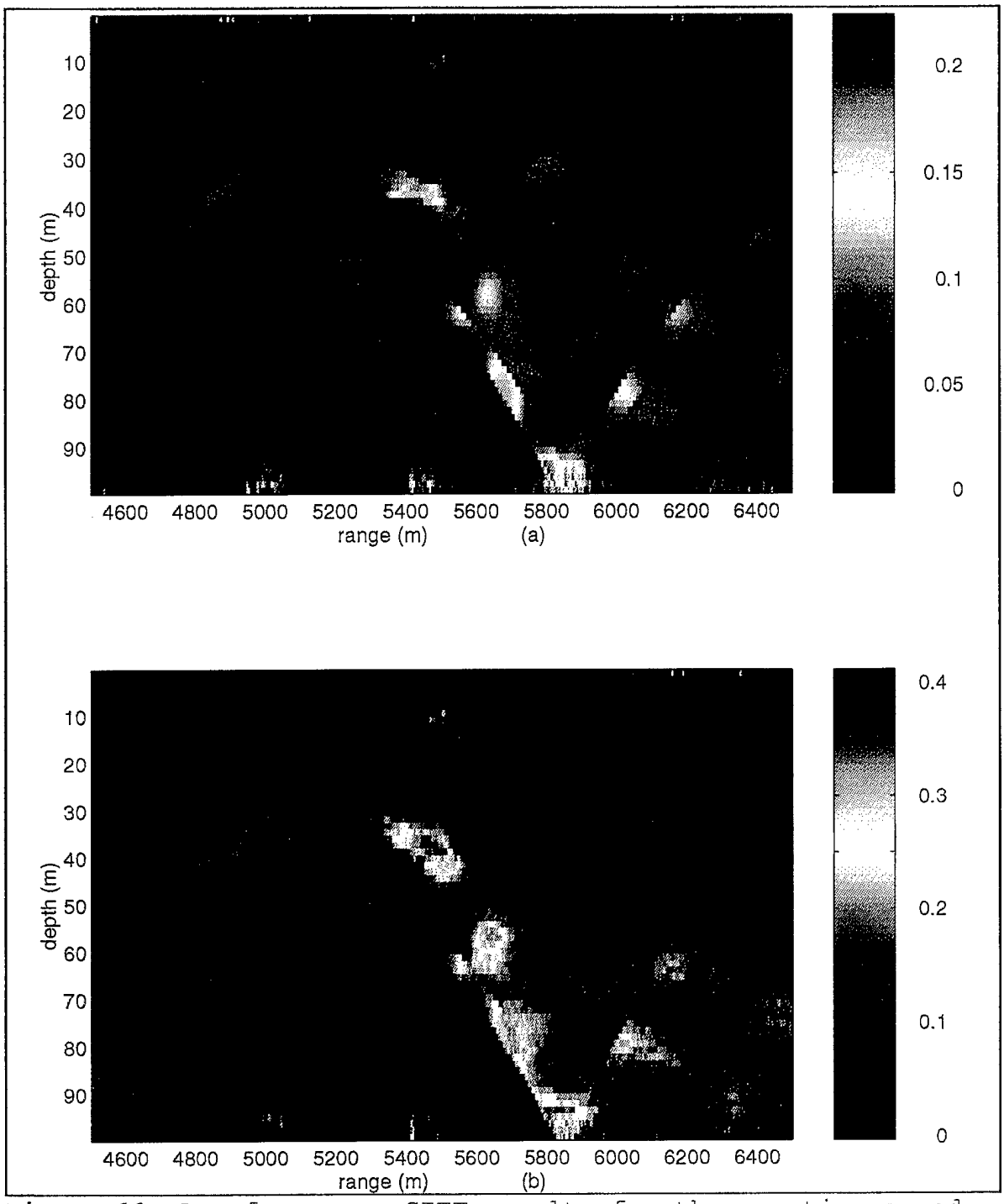

Figure 11 Low frequency SIFT results for the negative sound speed gradient environment using the 3-point SIFT algorithm and 250 Hz bandwidth. The scattered match results from working beyond the performance limitations. (a) Without add and compare approach applied. (b) With add and compare approach applied.

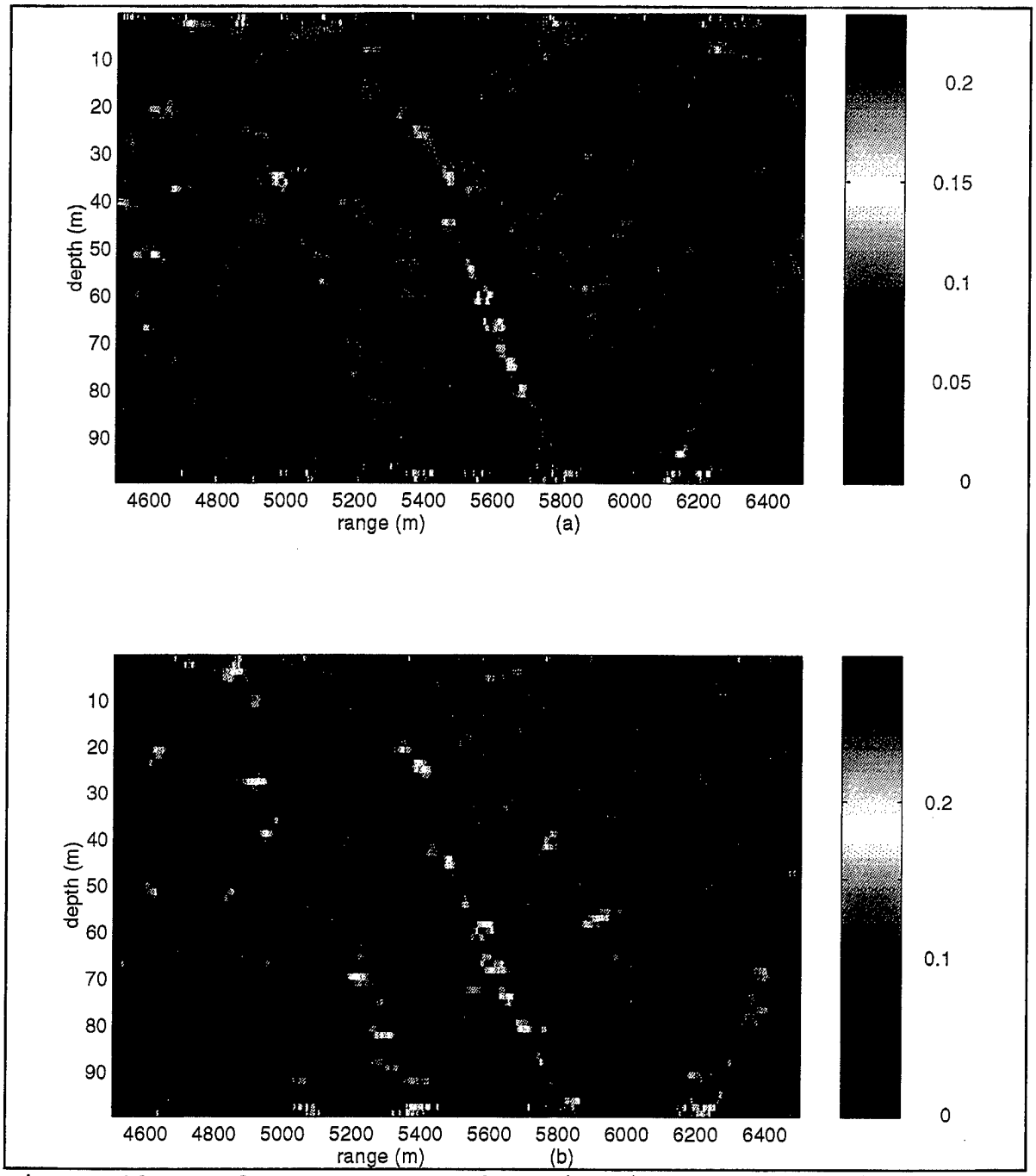

Figure 12 HF frequency SIFT localization results using a PE generated source, located at 5500 m range and 59.8 m depth and a receiver located at 40.2 m depth, for a negative soundspeed gradient environment. (a) 1-point SIFT algorithm, bandwidth 500 Hz, no window applied. Add and compare approach enhances the result. (b) 3-point SIFT algorithm, 500 Hz bandwidth, with Blackman window. Add and compare approach enhances the result.

V. SUGGESTIONS FOR FUTURE RESEARCH AND PRELIMINARY ANALYSIS OF OTHER MATCHING ALGORITHMS

Directions for future research for single hydrophone Matched Field Processing is one of the goals of this research. Some of the suggestions for future research may be slight modifications and improvements to existing algorithms. Those suggestions and their motivation have already been mentioned with the description of the algorithms in Chapter 3 and the analysis and results in Chapter 4. In this chapter, suggestions for more fundamental changes to existing algorithms and new algorithms are given.

A. SOURCE DEPENDENCE

The dependence on the source spectrum has been neglected throughout this research. If the source is a single, broadband, pulse-like transient, the specific details of the spectrum may not be critically important. A standard practice may be to filter out some portion of the signal spectrum over which all the processing will be done. An algorithm which is fairly insensitive to the spectral details is then needed.

However, if the source is composed of two or more closely spaced pulse-like events, the separation of the various multipaths at the receiver location becomes a formidable task. At issue then is whether a localization algorithm can be effective when utilizing only snippets of the arrival (i.e., portions of the signal believed to contain multipaths from a

single pulse-like event). Presumably, this is true if enough single event multipath information is available for analysis. The degradation of the localization due to multipath information needs to be investigated further.

B. MATCHING THE TIME-DOMAIN ARRIVAL STRUCTURES

Earlier analysis which directly compared arrival structures indicated that this coherent approach is too sensitive to phase errors. The autocorrelation matching technique also suffers from phase errors in the phase differences between separate arrivals. This suggests that we first remove all phase information by taking the absolute value of the basebanded, time-domain arrival structure. In order to emphasize the smaller amplitude of later arrivals, it might also be beneficial to then apply a high-pass filter in the frequency domain to remove the mean and low-order trends from the time-domain, absolute value arrival structure. On this signal you can apply the standard autocorrelation matching or just apply a normalized cross-correlation with a replica to perform the matching. Careful design of the high-pass filter is required, however, due to the transient response of the filter in the time-domain (The large peak in the arrival structure due to the initial arrivals triggers a large transient response). Figs. 13 (a) and 13 (b) show the absolute value of the arrival structure and the demoduted signal.

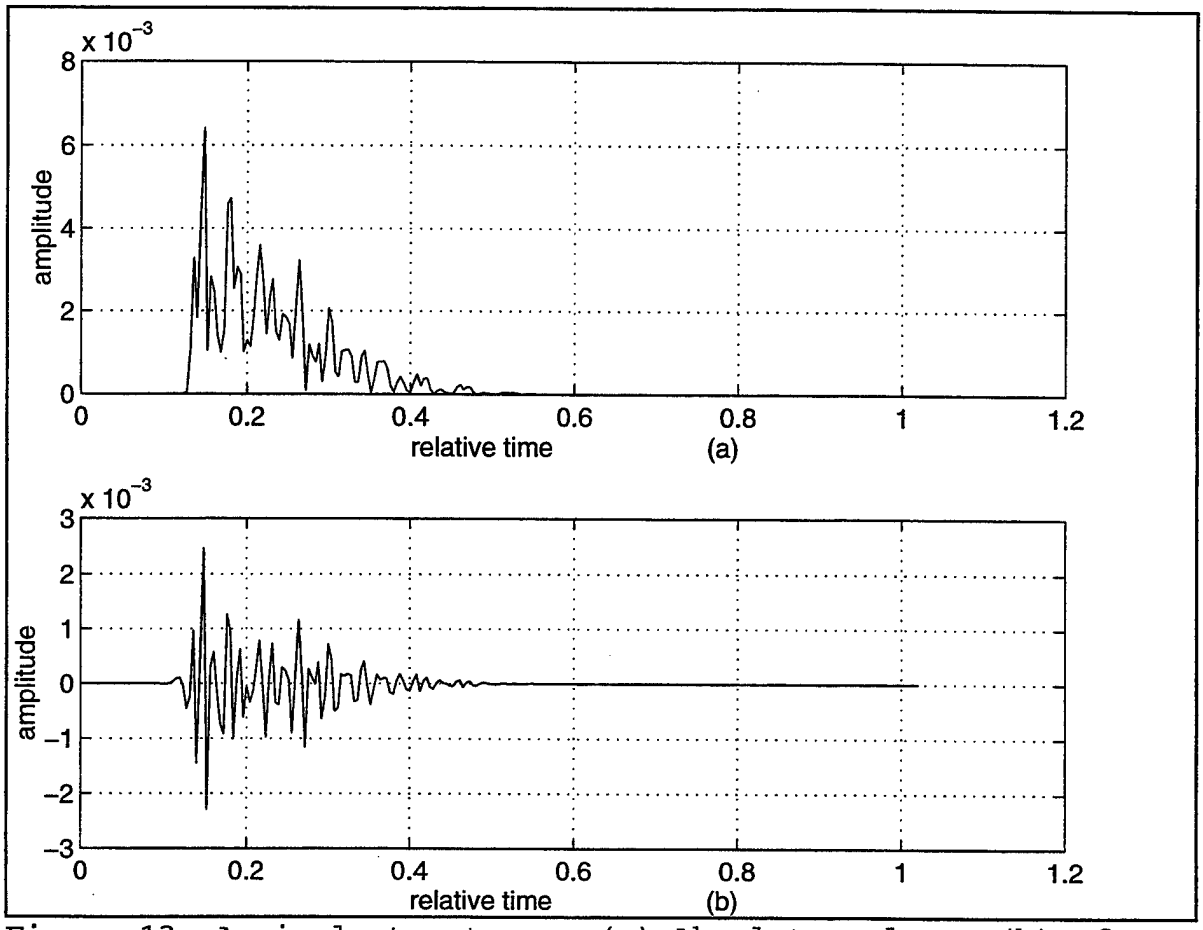

Figure 13 Arrival structure. (a) Absolute value. (b) After high-pass filtering.

A limited initial analysis has been done with some success. As the problem requires a specific filter which creates a minimum of phase and amplitude distortion a low coefficient Butterworth zero phase filter algorithm has been used. For the complete range in the iso-speed and negative gradient environment, a filter with 2 coefficients (effectively 4 coefficients due to the zero phase filter algorithm) and a cutoff of 0.3 times the Nyquist frequency using a sampling frequency of 250 Hz gave reasonable results. (Nb. The cutoff is related to the bandwidth and the sampling frequency). As the parameters of the matching algorithm have not been tuned to optimum performance, results may change a little after tuning of the parameters (e.g. number of notched lag values).

For autocorrelation matching, the baseline result using a negative gradient environment gives a footprint at 5500 m which is 80 cm in depth and approximately 40 m in range. Using a coherent match, the footprint becomes slightly larger in range and considerably larger in depth, approximately 120 cm in depth and 40 m range. Sidelobe levels are, however, considerably higher than for standard autocorrelation matching or coherent matching. Preliminary results using a ray code based template show that the direct match (normalized cross correlation) and the autocorrelation may perform very well for some source locations, while for other source locations performance may degrade severely due to high sidelobes. All footprints were found to be very small in depth.

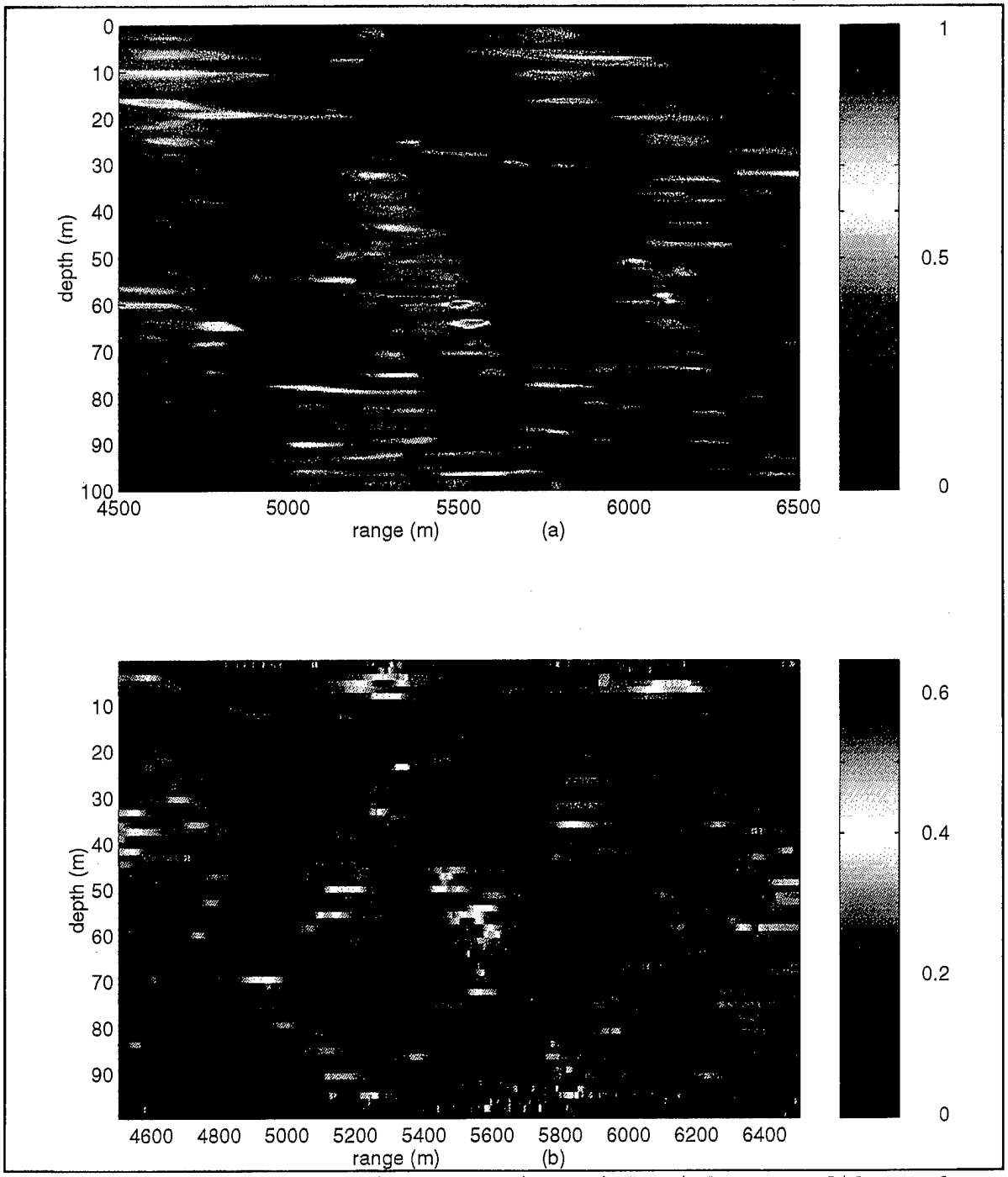

Figure 14 Autocorrelation matching with high-pass filtered arrival structures for the negative sound speed gradient environment. (a) Baseline result, for a source at 5500 m range and 59.8m depth and a receiver at 40.2 m depth. Note the high sidelobes and the large footprint. (b) Results using a PE generated source signal and ray code generated templates. There are small localization errors in range and depth.

It has been shown that the sample rate has a significant influence on the results. For the iso-speed environment, similar results have been found. The footprints for this environment are, however, larger. Combining this approach with a SIFT-like 1-point approximation algorithm did not perform well. This approach only relies on arrival times and completely neglects the phase and frequency for making the templates.

C. PARAMETRIZATION OF THE TIME-DOMAIN ARRIVAL STRUCTURE

Although originally not incorporated in the project, some analysis has been done with parametrization of the arrival structures and the replicas. As the arrival structures decay rapidly, it was suggested that they could be modeled as an auto regressive process. For the analysis, linear prediction coefficients were used and the Euclidian distance was used as a matching criterion. Results of the matching suggested that matching is possible without having to align the signals. Taking it a bit further would suggest that the same approach could be applied to one side of the autocorrelation function.

A limited preliminary analysis of the results has been performed. The scale used to present the results is log(1/D) where D is the euclidian distance. The matching works like a signature. The baseline footprint is very small, 1 resolution cell (5 m x 40 cm). A limited analysis of the robustness has been done using a random uniform 20% disturbance of the amplitudes of the frequency bins of the PE results. The match will stretch in range to 2-5 resolution cells and 2 resolution cells in depth. The algorithm works better for a low number

of coefficients. At a range of 5500 m for the negative gradient environment, performance is severely degraded using more than 10 coefficients which suggests that the description of the signals must not be too detailed. No phase perturbations have been tested. It is assumed that this might more severely degrade the performance. Using a PE generated source signal and ray code generated templates the algorithm still localizes but is severely degraded by high sidelobes. This preliminary analysis has only been performed in the 4500-6500 m range.

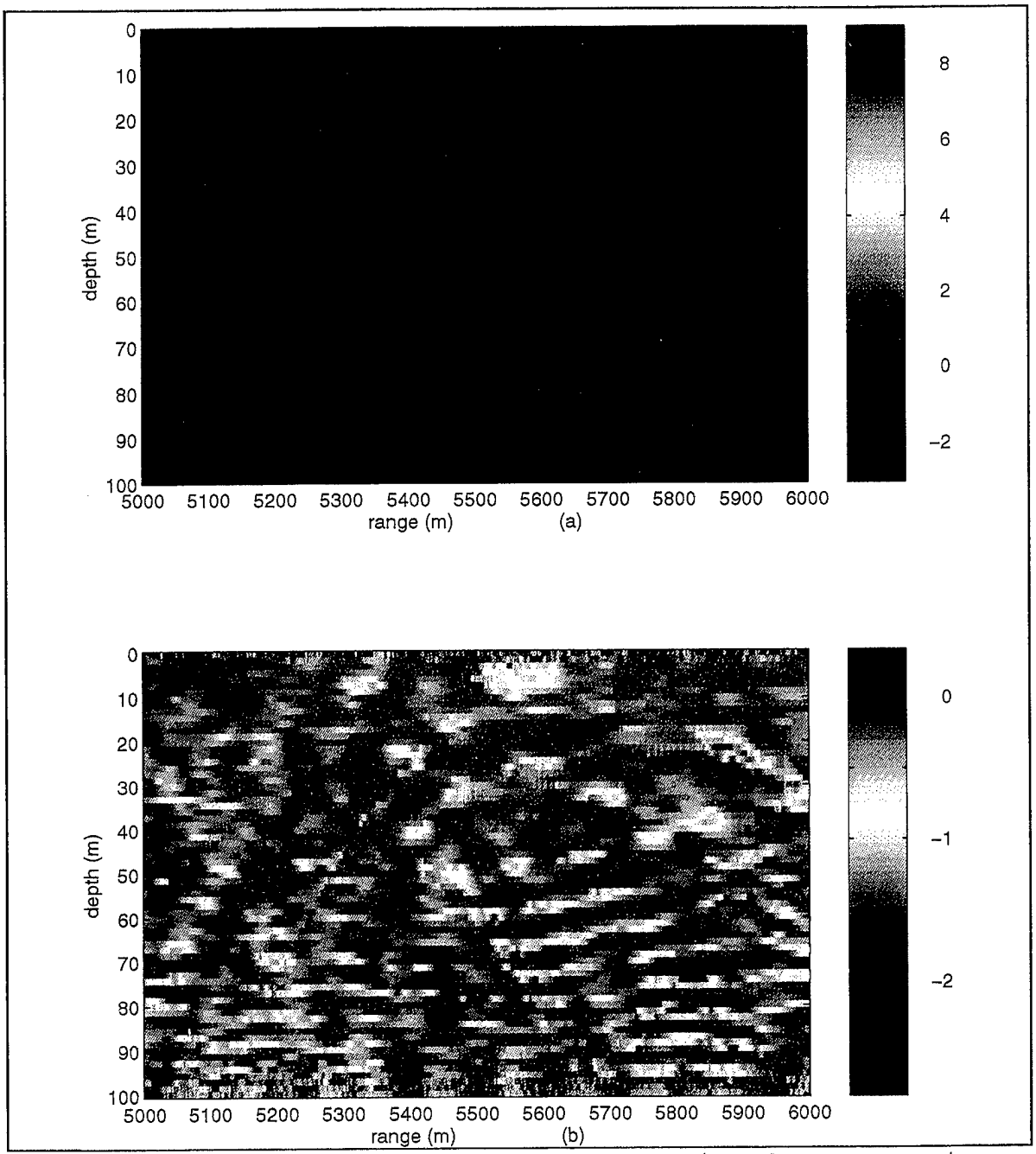

Figure 15 Results for parameterized matching for a negative sound speed gradient environment, where arrival structures are represented by 7 linear prediction coefficients. (a) Baseline results, for source located at 5500 m range and 59.8 m depth, and receiver at 40.2 m depth. The results is hardly visible as the match works like a signature and measures only one resolution cell. (b) Results using a PE generated source and ray code templates. Note the high sidelobes.

D. AUTOCORRELATION MATCHING OF THE FREQUENCY DOMAIN RESPONSE

The received signal shows a particular signature in the time domain as well as in the frequency domain due to the multipath interference. Note that the absolute value of the time-domain arrival structure described above is related to the autocorrelation of the frequency domain response through a Fourier transform by

$$G_{RR}(f) = \int_{-\infty}^{\infty} R(\chi)R^*(f+\chi)d\chi$$
$$= \int_{-\infty}^{\infty} R(t)R^*(t)e^{-i2\pi ft}dt. \quad \textbf{(93)}$$

A frequency-domain autocorrelation matching algorithm similar to the time-domain approach would then produce an ambiguity surface. The autocorrelation matching can now be formulated as

$$A = \int_{-\infty}^{\infty} G_{RR}^*(f)G_{PP}(f)df \quad \textbf{(94)}$$

and we can again notch out values near zero "lag" to remove the mean and low-order trends of the time domain. Note that this technique is essentially equivalent to matching the absolute value of the time-domain arrival structures.

Formulating the matching of the autocorrelation of the frequency response, however, has reintroduced the problem of defining an absolute reference time. In the definition of the replica autocorrelation, it is therefore necessary to introduce a free parameter to allow for searching in the time domain, i.e.,

$$\begin{aligned} G_{PP}(f,\tau) &= \int_{-\infty}^{\infty} p(t-\tau)p^*(t-\tau)e^{-i2\pi ft}dt \\ &= \int_{-\infty}^{\infty} p(t')p^*(t')e^{-i2\pi f(t'+\tau)}dt' \\ &= e^{-i2\pi f\tau}\int_{-\infty}^{\infty} P(\chi)P^*(\chi+f)df. \end{aligned} \tag{95}$$

The autocorrelation matching would now look like

$$A(\tau) = \int_{-\infty}^{\infty} G_{RR}^*(f)G_{PP}(f,\tau)df. \tag{96}$$

The values used for the ambiguity surface are now the values of $A(\tau)$ for which A is maximum. Furthermore, this algorithm applies to both real and complex signals, an improvement over the original SIFT design.

It should be noted that, while we developed this idea independently, it was recently brought to our attention that other investigators have previously used an extremely similar approach with reasonable success (Nghiem-Phu et al., 1992). We believe they were the first to suggest using this approach for this problem. However, they did not apply any of the filtering techniques we have suggested and improvements to their original concepts may still be forthcoming.

VI. CONCLUSIONS

Results of autocorrelation matching and approximate autocorrelation matching at the primary range of interest (5-10 km) proved to be highly inconsistent and sensitive to signal mismatch between ray-based methods and full-wave techniques. Due to our inability to generate data in the 2-4.5 km range for the negative sound speed gradient environment, only limited conclusions can be drawn from the results. The autocorrelation matching results appear to be bandwidth limited for longer ranges and limited by the sidelobe levels for shorter ranges. Results suggest that using the full 250 Hz bandwidth without windowing can lead to succesfull localization at ranges of more than 5 km. Footprint sizes are very small in depth (< 1 m) and moderately small in range (<15 m). Taking into account phase differences in the autocorrelations improves the peak to sidelobe levels. Notching out values near zero lag improves the dynamic range and reduces the chance of invalid localizations (due to energy matching instead of shape matching) but reduces the footprint size. Results for the iso-speed environment are much better, as may be expected, and footprints are larger than for the negative gradient environment.

The SIFT algorithm is very sensitive and more bandwidth limited than the autocorrelation matching. For the low frequency version of the algorithm, a first order description of performance limitations is suggested. The high frequency versions of the algorithm did not give consistent results for the negative gradient environment in either the 750-1000 Hz or the 500-1000 Hz band but proved to work well in the iso-speed

environment. The high frequency versions seem to be even more bandwitdh limited than the low frequency versions and thereby severly reduces the range of applicability. Results suggest that localization can be performed at ranges less than 5 km for a bandwidth of 250 Hz and a bottom depth of 100 m and moderate sound speed gradient environments. Using a large bandwidth 'localization by sidelobes' could be performed in some cases but with minimal resolution. Finally, additional improvements may be achieved for the negative gradient environment by taking into account the phase shift in the 'half' matching autocorrelation results, using no window (thereby using the full bandwidth) and extending the range to include the 2-4.5 km bracket. The same approach may improve the SIFT results where the multi-point approach may also be considered.

APPENDIX : SPATIAL BEAMFORMING AS A FORM OF MFP

The autocorrelation matching in the frequency domain can be related to a generalized and normalized Bartlett beamformer. The main difference is the neglect of the off diagonal terms in the correlation matrix of the frequency domain received signal. This is closely related to the fact mentioned by Miller et al. (1996) that the correlation-based algorithms are likely to work better on noise-like signals than on sinusoidally signals.

The approach presented here is an analogue of the spatial techniques known in beamforming and frequency bank techniques known in spectral estimation. In most applications of Matched Field Processing (MFP), an array of receiver hydrophones is used. The output of the beamformer for the standard Bartlett beamformer is then defined as

$$B_B=E\{|b(t)|^2\}=w_\theta^H R_p w_\theta=w^H E\{p(t)p^H(t)\}w_0 \qquad \textbf{(97)}$$

where R_p is the matrix of the data $p(t)$, and w is the weighting vector for a particular look direction. The data $p(t)$ can be defined as

$$p_i(t)=a_i(\theta_l)s_l(t)+n_i(t) \qquad i=1,.....,N, \qquad \textbf{(98)}$$

where N is the number of elements in the array, $n(t)$ is the noise, $a_i(\theta_l)$ is the array response for a source in the direction θ_l and $s_l(t)$ is the source function for a source in direction θ_l. Usually this approach is based on the plane wave approximation, and the beamformer can be refined to multi-variance, multiple constraint or more exotic schemes. The step from

plane wave beamforming to MFP is made by including the knowledge of the environment and the propagation, usually by means of a propagation model, in the weighting vectors. This enables you to make estimates in more dimensions, usually a 2-D range/depth plane. Necessary for this generalized beamforming to work is that the description of the environment and the propagation is accurate enough, the environment has enough variation over the distances of interest, and the weight vectors at different points are different enough to form a consistent match. In MFP the weighting vectors are usually called replicas and the generalized beamformers are called processors. The most common are the Bartlett, the multi-variance and the multiple constraint processors,

$$\begin{aligned} B_B &= \underline{w}^H R_P \underline{w}, \\ B_{MV} &= \left[\underline{w}^H R_P^{-1} \underline{w}\right]^{-1}, \\ B_{MCM} &= \underline{c}^H \left[W^H R_P^{-1} W\right]^{-1} \underline{c}, \end{aligned} \tag{99}$$

where W is the matrix of the replica vectors defining the multiple constraints around the look direction. The elements of $\underline{c}$ are defined by

$$c_m = \underline{w}_l^H \underline{w}_m \tag{100}$$

where $\underline{w}_l$ is the replica vector in the look direction and $\underline{w}_m$ are the vectors defining the constraints.

The above spatial approach can be applied to a broadband time domain signal using one hydrophone instead of the spatial array. Two different approaches will be shown, one

in the time domain and one in the frequency domain. We define the preenvelope (or complex envelope of the signal) of the received pressure as

$$\tilde{p}(t_i)=\tilde{a}\tilde{s}(t_i)+\tilde{n}(t_i) \qquad i=1,.....,N, \tag{101}$$

where $\tilde{a}$ is the complex response of a hydrophone to a source at location (r_s, z_s) to a complex source at time t_i. The Bartlett processor can be formulated as

$$B_B=\underline{w}^H R_p \underline{w} \tag{102}$$

where $\underline{w}$ are the replicas. The problem with this time-domain approach is the lack of a time reference for the replicas. With an array, all the hydrophone locations are assumed known and provide a reference in space. The reference in time is not so easy to establish. Unless you can overcome this problem, this approach does not seem viable

On the other hand, taking the second frequency-domain approach a proper absolute time reference can be established. Define the frequency domain received pressure as

$$\tilde{p}(f_i)=\tilde{a}\tilde{s}(f_i)+\tilde{n}(f_i). \tag{103}$$

Treating it the same way as the spatial array R_p can then be defined by

$$\begin{aligned} R_{\tilde{p}} &= \{\underline{\tilde{p}}(f)\ \underline{\tilde{p}}^H(f)\} \\ &= E\{\tilde{a}\ \underline{\tilde{s}}(f)\underline{\tilde{s}}^H(f)\tilde{a}^H+\underline{\tilde{n}}(f)\underline{\tilde{n}}^H(f)\}. \end{aligned} \tag{104}$$

The generalized 'beamformer' or matching algorithms can be defined as

$$B_B = \underline{\tilde{w}}^H R_{\underline{p}} \underline{\tilde{w}}. \tag{105}$$

This approach does not encounter the reference problems an approach in the time domain would have. This approach could also be extended to other types of processors. The Bartlett processor is closely related to autocorrelation matching. If we define the autocorrelation matching in the frequency domain as

$$A = \frac{\sum G_{RR}(f) G_{TT}(f)}{\sqrt{\sum |G_{RR}(f)|^2 \sum |G_{TT}(f)|^2}}, \tag{106}$$

it is clear that this looks like a normalized Bartlett processor where the off diagonal terms have been neglected.

LIST OF REFERENCES

Bendat J. S., Piersol A. G., *Random Data: Analysis and Measurement Procedures*, Wiley-Interscience, New York, 1971.

Benson J. L., *Time-Domain Localization of Transient Source in Shallow Water*, Naval Post Graduate School M.S. Thesis, June 1995.

Harris F. J., *"On the Use of Windows for Harmonic Analysis with the Discrete Fourier Transform"*, Proc. IEEE, vol. 66 no. 1, January 1978.

Jensen F. B., Kuperman W. A., Porter M. B., Schmidt H., *Computational Ocean Acoustics*, American Institute of Physics Press, 1994.

Jones R. M., Riley J. P., Georges T. M., *HARPO - a versatile three dimensional Hamiltonian ray tracing program for acoustic wave in the ocean with irregular bottom*, NOAA Wave Propagation Laboratory Report, October 1986.

Kinsler L. E., Frey R. F., *Fundamentals of acoustics*, John Wiley & Sons, 1962.

Lighthill, M. J., *Waves in Fluids*, Cambridge University Press, 1978.

Miller J. H., Benson J. L., Chiu C-S., Smith K. B., *Transient Localization Project at the NPS, Fiscal Year 1995 results*, Naval Postgraduate School, April 1996.

Nhgiem-Phu L., Tappert F. D., Carle H. M., *Broadband Matched Field Processing (BMFP) Using Incoherent and Semi-coherent Techniques with Ray-Based Green's function*, Mac Systems Corp. Technical Report no. TR 07-92, 16 Nov.. 1992.

Pierce D. D., *Range-dependant Passive Source Localization using data from the Barents Sea Tomography experiment*, Ph.D. dissertation, Naval Postgraduate School, Monterey.

Smith K.B., Brown M. G., and Tappert F. D.,*"Ray chaos in underwater acoustics,"*, J. Acoust. Soc. Am. 91, 1939-1949, 1992.

Smith K. B., Tappert F. D., *UMPE: The University of Miami Parabolic Equation Model version 1.1*, MPL Technical Memorandum 432 May 1993 (revised edition September 1994), Marine Physical Laboratory, Scripps Institution of Oceanography, University of San Diego

Tappert F. D., "Parabolic equation method", in Lecture Notes in Physics, Vol. 70, Wave Propagation and Underwater Acoustics, pp. 224-287, edited by J. B. Keller and J. S. Papadakis, Springer Verlag, New York, 1977.

Therrien C. W., *Discrete Random signals and Statistical Signal Processing,* Prentice Hall, 1992.

Thomson D. J., Chapman N. R., "A wide-angle split step algorithm for the parabolic equation models", JASA Suppl. 1 83, 1988.

Ziomek L. J., *Acoustic Field Theory and Space-Time Signal Processing,* CRC Press, 1995

INITIAL DISTRIBUTION LIST

	No. Copies
1. Defense Technical Information Center 8725 John J. Kingman Rd., STE 0944 Ft. Belvoir, VA 22060-6218	2
2. Dudley Knox Library Naval Postgraduate School 411 Dyer Rd. Monterey, CA 93943-5101	2
3. Dr. Kevin B. Smith Physics Department Naval Postgraduate School Monterey, CA 93943-5122	2
4. Dr. Ching-Sang Chiu Oceanography Department Naval Postgraduate School Monterey, CA 93943-5122	1
5. Stephen Greineder Naval Undersea Warfare Center, Division Newport Code 2121, Bldg 1320, Room 380 Newport, RI 02841	2